CHAPTER V

Kinetic studies on redox reactions between Na_2SO_3 and dioxouranium (VI) complexes with chiral aldimine ligands derived from L–/ D – asparagine, arginine and glutamine; crystal structure of (2,2′ - bipyridyl) dioxo (N – salicylidene – L – asparaginato) uranium (VI) – methanol (1/1).

Abstract

Kinetic data of redox reactions between Na_2SO_3 and several well-characterized dioxouranium (VI) / uranyl complexes with chiral aldimine ligands, possessing L – and D – asparagine, arginine and glutamine, have been recorded spectrophotometrically. [UO_2 (S – L – Asn)(bipy)]. CH_3OH [compound (**2**)] crystallizes in the orthorhombic space group P 2_1 2_1 2_1 with a = 7.179 (3) Å, b = 13.437 (5) Å, c = 23.812 (8) Å and z = 4. The essentially linear UO_2^{2+} entity [O(1) – U(1) – O(2) = 176.0 $(3)^0$] achieves an equatorial coordination number of five involving the tridentate aldimine ligand anion (S–L –Asn^{2-}) and the neutral bidentate donor (bipy). Chemical compositions of other complexes have been verified through simulation of mass spectral data. The above reactions follow second – order rate law in DMSO – H_2O (3 : 2 v/v) at 290 K. For complex (3) at 288 K the one – electron reduction product, that is, the UO_2^+ entity could be identified in the available time – scale and this view is supported by electrochemical data (e.g., cyclic voltammetry and controlled – potential coulometry). A comparative study of the kinetic data reveals the dependence of k_{obs} (s^{-1}) values on the chemical composition of the complexes, especially the nature of R group of amino acid residue and the associated stereochemistry around the C_α atom (that is, relative positions of the H_α atom and the R group as evident from chiroptical studies).

Introduction

In this Chapter, the attention is focussed on the reactivity of chiral coordination compounds of UO_2^{2+} entity with aldimine ligands [Scheme (V-1)], towards a suitable reducing agent like Na_2SO_3 and analyzing the kinetic data on the basis of different characteristic aspects of the chiral aldimine ligands and the M → L π – bonding ability of the secondary ligands (2,2′ – bipyridyl / 1,10 – phenanthroline).

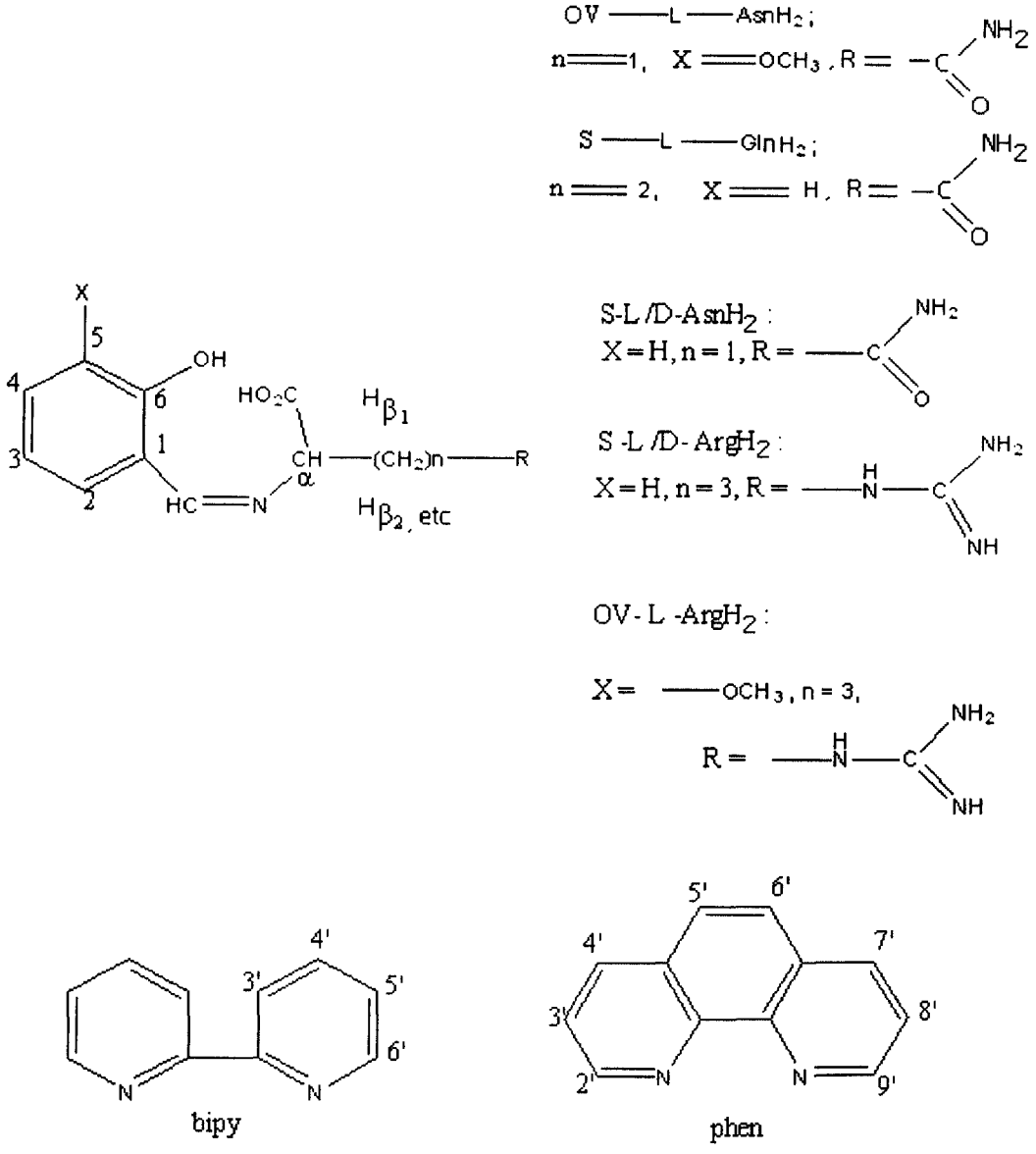

Scheme (V – 1): Schematic formulae of aldimine ligands.

In the earlier Chapters coordination Chemistry of molybdenum in the oxidation states VI, V and IV has been discussed ; some of them contain the characteristic attribute of an oxomatal entity, that is, the multiply bonded oxygen atom stabilizing the high charge on the metal atom. As pointed out in Chapter I, molybdenum in its higher oxidation states (VI, V, IV) can form a wide variety of oxometal entities, many of which have been characterized structurally [55]. This ability can be correlated with the fact that molybdenum is not as "oxophilic" as the early transition metals of groups IV and V. Its strong tendency to bind an oxo group (= O) is balanced by a capacity to lose a single oxygen atom easily ; this is accompanied by changes in oxidation states (VI, V, IV) of the molybdenum atom [41].

However, for the dioxouranium (VI) / uranyl (UO_2^{2+}) ion, the situation is quite different. The linear UO_2^{2+} ion is remarkably stable with respect to the strength of the U – O bond and it can persist through a variety of chemical changes and behaves like a cation with properties intermediate between those of M^+ and M^{2+} ions of similar size but greater charge [141, 165]. The UO_2^{2+} ion readily adds 4 – 6 donor atoms in its equatorial plane to give structures which range from octahedral to hexagonal bipyramidal, through pentagonal bipyramidal with overall coordination number of 6 – 8 for the central U(VI) atom ; the number of known complexes is vast involving oxygen, nitrogen and even sulphur donor ligands [141]. In spite of all these developments, specific areas of Chemistry of the UO_2^{2+} ion still continues to arouse avid interest as stated below. Both experimental and theoretical methods have been used to study UO_2^{2+} compounds in terms of their structural, electronic, spectroscopic and thermochemical properties [166 – 169].

The rich coordination Chemistry of the UO_2^{2+} ion shows continued growth in specific directions [105, 170 – 173].

Here several coordination compounds of the UO_2^{2+} entity with aldimine ligands, possessing L – and D – arginine / asparagine / glutamine residues [Scheme (V–1)] have been found to be excellent candidates for kinetic studies with a suitable reducing agent, e.g., Na_2SO_3 in DMSO – H_2O (3 : 2 v/v) medium. Although they have been available from a previous synthesis [146], one of them have been further characterized

structurally through X – ray crystallographically in this work ; in other cases, the assignments of chemical compositions have been verified through mass spectrometry. Importance of the aldimine ligands containing amino acid residues is well – known [74, 93]. The objectives of this study involving the UO_2^{2+} ion is outlined below.

The U – O bonding (of UO_2^{2+} ion) can be formulated with a scheme in which appropriate d and f orbitals can be combined into MOs to give one σ plus two π bonds [103, 168]. The MOs are filled at UO_2^{2+} and succeeding electrons are fed into non – bonding orbitals ; the MO scheme is helpful for interpretation of spectroscopic and other data. For example, the reduction $UO_2^{2+} \rightarrow UO_2^{+}$ involves feeding one electron into either of the uranium – centred nonbonding 1 δ_u or 1 ϕ_u orbitals which have pure atomic 5f character [103, 168] ; this process involves elongation of the U – O bond and it destabilizes the UO_2^{+} ion considerably [168]. As a result, aqueous Chemistry of the UO_2^{+} ion could be studied only by special techniques (e. g., stopped – flow method) ; in DMSO it is more stable, both thermodynamically and kinetically [141, 165]. Besides this, involvement of the UO_2^{+} intermediate has been indicated in UO_2^{2+} catalysed photooxidation of either hydrocarbons with molecular oxygen or aromatic hydrocarbons by H_2O_2 [176, 177]. The decay of the excited uranyl ion in water in presence of halide ions has been studied by laser flash kinetic spectrophotometry[178]; the proposed mechanism for effective quenching of the green luminescence of uranyl ion by halides involves the intermediate formation of the short – lived UO_2^{+} ion.

On the other hand, U(IV) ion has greater stability and it can be obtained by the reduction of the UO_2^{2+} ion with a strong reducing agent like a silver reductor or by Cr^{2+} [25].

It will be interesting to follow the redox Chemistry of the present uranyl complexes with aldimine ligands, involving stepwise conversion of the UO_2^{2+} species to UO_2^{+} and finally to U(IV) state, which are related by the following redox couples (formal reduction potential in volts are shown) [165] :

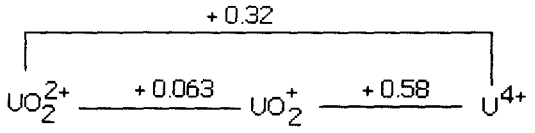

Here, UO_2^{2+} ion is the most stable species, whereas UO_2^{+} ion is the least stable one. The redox couple involving oxygen atom transfer, e.g.,

$$UO_2^{2+} + 4H^+ + 2e^- = U^{4+} + 2H_2O,$$

is irreversible, whereas a couple like $UO_2^{2+} + e^- = UO_2^{+}$ should be reversible, at least for a brief time scale, as permitted by the life – time of the UO_2^{+} ion. The aim of this study is to utilize a milder reducing agent (than silver reductor or Cr^{2+}) like Na_2SO_3 in DMSO – H_2O medium towards the present uranyl – aldimine complexes, to explore whether the short – lived UO_2^{+} intermediate could be formed at least for a time duration for recording the kinetic data in the time - scale of a conventional recording UV – VIS spectrophotometer.

The reducing character of SO_3^{2-} ion is expressed quantitatively as follows [165] :

$$SO_4^{2-} + H_2O + 2e^- = SO_3^{2-} + 2OH^-, \quad E^o = -0.93 \text{ V}.$$

In aqueous medium the oxidation of SO_3^{2-} to SO_4^{2-} can be carried out by both one – electron and two – electron oxidants like Fe^{3+} ion and Cl_2 respectively [165]. In view of the above, both the UO_2^{+} and U(IV) states should be attainable through stepwise reduction of UO_2^{2+} ion by SO_3^{2-}. The final requirement is the presence of a compact ligand donor set on the equatorial plane of the linear UO_2^{2+} entity with M → L π bonding ability [155], so that increased size of the UO_2^{+} entity accompanying the electron transfer step :

$$UO_2^{2+} + e^- \rightarrow UO_2^{+} \text{ -----(1)}$$

could be partly counter balanced, for a time duration needed for the pertinent measurements. The kinetic data recorded here throw light on the interesting aspects of this study. Reaction stoichiometry measurement (as stated here) indicated the following overall reaction :

$$U^{VI}O_2^{2+} + S^{IV}O_3^{2-} + H_2O \rightarrow U^{4+} + S^{VI}O_4^{2-} + 2\,OH^- \text{ -----(2)}$$

Experimental

Materials and Methods : Ortho –Vanilline (Fluka), salicylaldehyde (Kemphasol), L – asparagine monohydrate (BDH, England), L – glutamine (BDH, England), L – and D – arginine monohydrochloride (Fluka), 2,2/ – bipyridyl (BDH), 1,10 – phenanthroline monohydrochloride (BDH) and uranyl nitrate hexahydrate GR (Loba, Bombay) were used as such. Bu_4NClO_4 was prepared from Bu_4NOH (SRL, Mumbai) following published method [11]. The solvents were purified by literature procedures [9].

Elemental analysis (C, H, N data), FAB mass spectra, ESIMS data, IR, UV – VIS, ^1H NMR, CD spectra and cyclic voltammetry data were recorded as described in earlier chapters. Uranium was estimated titrimetrically [175]. Kinetic measurement in DMSO – H_2O (3 : 2 v/v) were carried out on a Shimadzu 160A UV – VIS spectrophotometer.

X – ray data collection and reduction :

A brick-red coloured orthorhombic crystal of $[UO_2(S - L - Asn)(bipy)].CH_3OH$ [compound **(2)**] was used for single crystal X – ray diffraction study at the Department of Chemistry, University of Helsinki, Finland, in collaboration with Prof. R. Hämäläinen. SHELXTL PC programs were used for this purpose. Structural refinement was done by using SHELXL – 93 programs. The basic conditions are stated in Table (V–1). The ORTEP diagram of the molecule is shown in Fig.(V–1) and the unit cell structure is shown in Fig.(V – 2). Bond lengths (Å) and bond angles (deg) data for compound (**2**) along with other X – ray crystallographic information are presented in Tables (V – 2) to (V – 5).

Table (V – 1): Crystal data and structure refinement for **(2)** :

Empirical formula	$C_{22}H_{22}N_4O_7U$
Formula weight (M)	692.47
Crystal system	Orthorhombic
Space group	$P2_12_12_1$
Unit cell dimensions	a = 7.179(3) Å.
	b =13.437(5) Å.
	c = 23.812(8) Å.
Volume	2297.0(15) A^ 3
z	4
D_m, D_c / Mg m^{-3}	2.03, 2.00
F(000)	1320
Diffractometer	Rigaku AFC – 7S
Monochromator	Graphite
Crystal size (mm)	0.25 x 0.15 x 0.05
Radiation	Mo/ Kα (λ 0.71069 Å)
μ (Mo / Kα) mm^{-1}	7.12
Orientation reflections	25
T / ^{0}C	– 80
Scan method, speed / ^{0} min^{-1}	ω , 5
h,k,l ranges	0 > h > - 9, 0 > k > -16, 0 > 1 > -29
Measured 2θ range / ^{0}	3.0 --53.0
Check reflections, variation (%)	3,3
No. measured reflections	2622
R (for 2619 data)	0.035
wR [w = 1/ σ^2(F) + 0.0024(F^2)]	0.046
Maximum Δ/σ	0.007
Maximum, minimum ρ in ΔF map/e $Å^{-3}$	1.12 – 1.43.

Synthesis

The uranyl complexes of aldimine ligands [(**2**) – (**6**)] involved in the present study were synthesized by standard procedures [146]. In most cases the aldimine ligands were obtained in – situ during the complex formation process ; however, in one case, e.g., complex (**6**), the monopotassium salt of N – (orthovanillidene) – L – asparagine (OV – L – AsnHK) (**1**) was isolated in the solid state and used for the synthesis giving better results.

Purity of the freshly synthesized ligand (**1**) and the complexes (**2** – **6**) was checked through TLC, elemental analysis, FABMS / ESIMS data and matching of the UV – VIS as well as IR spectral data with the original ones. For TLC purposes, the compounds were dissolved in CH_3OH for spotting the plates (silica gel G with iodine chamber for detection) and absolute ethanol was used as the eluant. Outlines of the synthetic procedures are stated below [146].

Monopotassium salt of N – (orthovanillidine)– L – asparagine (OV–L–AsnHK) (1)

L – asparagine monohydrate (1 mmol) dissolved in 10 ml of methanolic KOH (1 mmol) + Orthovanillin (1 mmol) in 10 ml of CH_3OH

↓ boiled under reflux for 30 min and allowed to settle

OV – L – AsnHK (**1**)

Orange – yellow crystals were washed thoroughly with CH_3OH, diethyl ether and dried in vacuo over anhy. $CaCl_2$; yield : 50 %.

The other free ligands like S – L – AsnHK. H_2O, S – L – $ArgH_2$ and OV – L – ArgHK could be synthesized by similar methods ; the purified products have been utilized for recording their ^1H NMR spectral data [Table (V – 6)].

$[UO_2(S - L - Asn)(bipy)].CH_3OH$ (2)

A solution of L – asparagine monohydrate (1 mmol) and KOH (1.5 ml) in 15 ml of $CH_3OH - H_2O$ (2 : 1 v/v)

+

A solution of salicylaldehyde (1 mmol) in CH_3OH (10 ml)

↓

To this in– situ ligand solution, the following reagents were added consecutively under stirring at 333 K.

$UO_2(NO_3)_2.6H_2O$ (1 mmol) in 10 ml of $CH_3OH - H_2O$ (1 : 1 v/v), followed by 2,2′ – bipyridyl (1 mmol) in 10 ml of CH_3OH. Final pH was 4.0. The brick – red compound was washed with $CH_3OH - H_2O$ (1 : 1 v/v), CH_3OH, diethyl ether and dried in vacuo over anhy. $CaCl_2$. Yield : 30 % (after recrystallization from CH_3OH).

X – ray quality crystals were obtained by recrystallizing the compound twice from CH_3OH water (4 : 1 v/v).

The following compounds could be synthesized by a similar procedure as above, using the appropriate amino acid and 1,10 – phenanthroline instead of 2,2′ – bipyridyl.

$[UO_2(S - L - Arg)(phen)].2H_2O$ (3)
(light rose – red coloured compound)

$[UO_2(S - D - Arg)(phen)].H_2O$ (3′)
(rose – red coloured compound)

$[UO_2(S - L - Gln)(phen)].H_2O$ (5)
(rosy – red coloured compound)

Schematic outlines of synthesis of complexes (**4**) and (**6**) are shown below [146].

K [UO_2(OV – L – Arg) (OV – L – ArgH)]. 4H_2O (4)

L – arginine monohydrochloride (2 mmol) dissolved in KOH (2 mmol) in 20 ml CH_3OH – H_2O (1 : 1 v/v) + Orthovanilline (2 mmol) in 10 ml CH_3OH

↓ addition of a solution of $UO_2(NO_3)_2 \cdot 6H_2O$ (1 mmol) in 5 ml H_2O under stirring at 343 K, final pH 4.3.

The dark – red compound separated on standing for 3h ; it was washed with CH_3OH – H_2O (1 : 1 v/v), CH_3OH, diethyl ether and dried in vacuo over anhy. $CaCl_2$. Yield : 45 %.

[(UO_2)$_2$ (OV – L – Asn)$_2$ (bipy)(H_2O)$_2$ (6)

To a solution of OV – L – AsnHK (1 mmol) in 15 ml CH_3OH, the following solutions were added consecutively under stirring at 333 K

↓

a solution of $UO_2(NO_3)_2.6H_2O$ (1 mmol) in 5 ml H_2O, followed by a solution of 2,2′ – bipyridyl (1 mmol) in 5 ml CH_3OH. The final pH was 4.5.

↓

The brown compound was obtained on allowing the reaction mixture to settle and it was worked up through the aforesaid sequence of manipulations. Yield : 55 %.

Results and Discussion

The molecular structure of (**2**) as shown in Figure (V – 1), is based on a mononuclear seven – coordinate uranium atom in pentagonal bipyramidal geometry. The tridentate coordination of the aldimine ligand is achieved by the phenoxide oxygen, imine nitrogen and one of the carbonyl oxygen atom ; the two nitrogen atoms of 2,2′ – bipyridyl occupy the remaining two corners of the equatorial coordination pentagon. The two apical oxygen atoms of the UO_2^{2+} entity complete the pentagonal bipyramid. The O – U – O axis shows a 4° deviation from linearity ; the two nitrogen atoms of

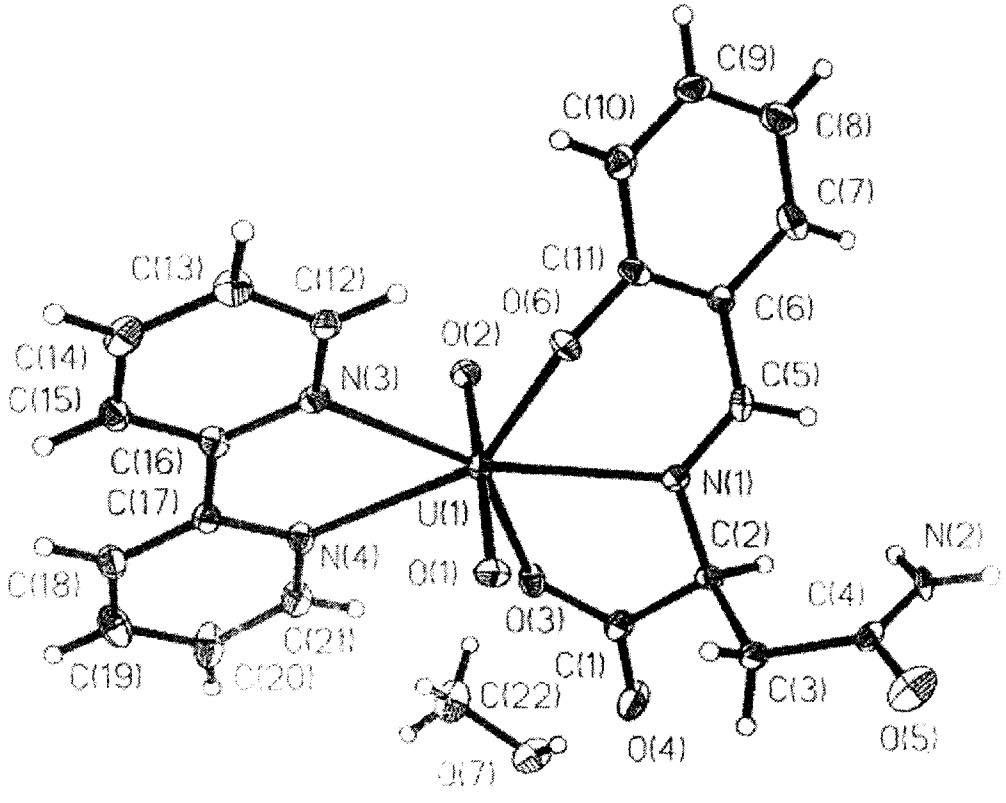

Fig.(V – 1): An ORTEP diagram of $[UO_2(S\text{–}L\text{–}Asn)(bipy)].CH_3OH$ (**2**) showing the atom – numbering scheme. Thermal ellipsoids represent 50 % probability.

2,2′ – bipyridyl have different U – N bond lengths. The bond angles data in Table (V – 2) throw light on the puckering of the equatorial chelate rings. The CH_3OH molecule forms a hydrogen bond with the carboxylate oxygen, O (4), where the O(7) to O(4) distance is 2.713 Å. Another interesting aspect is that the amide nitrogen atom, N(2) is not involved in coordination with the metal centre.

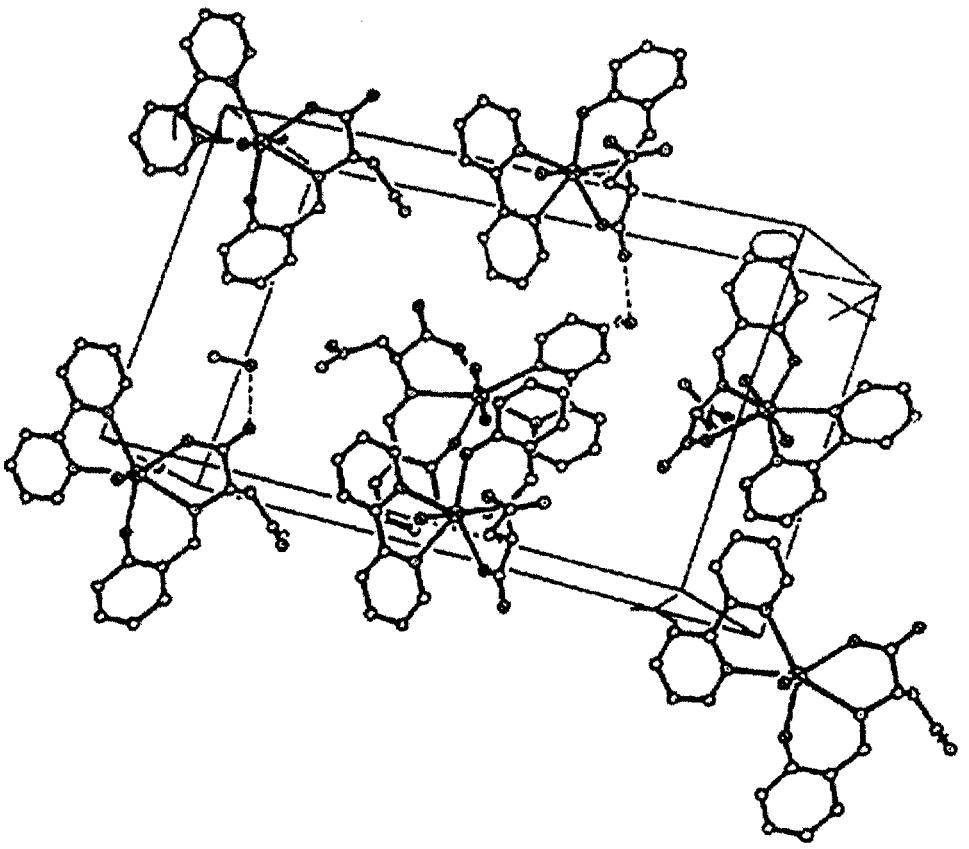

Fig.(V – 2): The unit cell structure of $[UO_2(S\text{-}L\text{-}Asn)(bipy)].\ CH_3OH$ (**2**) crystal.

Table (V – 2): Bond lengths [Å] and bond angles [deg.] for compound (**2**)

U1 --- 01	1.772(7)	C10 --- C11	1.423 (14)
U1 --- 02	1.764 (7)	C12 --- C13	1.380 (15)
U1 --- 03	2.369 (7)	C13 --- C14	1.371 (15)
U1 --- 06	2.214 (6)	C14 --- C15	1.388 (15)
U1 --- N1	2.505 (7)	C15 --- C16	1.405 (14)
U1 --- N3	2.563 (8)	C16 --- C17	1.496 (13)
U1 --- N4	2.577 (8)	C17 --- C18	1.391 (13)
O3 --- C1	1.287 (12)	C18 --- C19	1.373 (15)
O4 --- C1	1.230 (13)	C19 --- C20	1.376 (17)
O5 --- C4	1.349 (12)	C20 --- C21	1.382 (16)
O6 --- C11	1.330 (11)		
O7 --- C22	1.390 (17)	O1---U1---O2	176.0 (3)
N1 --- C2	1.468 (12)	O1---U1---O3	88.9 (3)
N1 --- C5	1.300 (12)	O2---U1---O3	88.1 (3)
N2 --- C4	1.232 (12)	O1---U1---O6	94.4 (3)

N3 --- C12	1.346 (12)	O2---U1---O6	89.5 (3)
N3 --- C16	1.344 (13)	O3---U1---O6	135.0 (2)
N4 --- C17	1.344 (12)	O1---U1---N1	89.2 (3)
N4 --- C21	1.352 (13)	O2---U1---N1	92.0 (3)
C1 --- C2	1.531 (13)	O3---U1---N1	64.3 (3)
C2 --- C3	1.536 (13)	O6---U1---N1	70.8 (3)
C3 --- C4	1.508 (14)	O6---U1---N3	81.2 (3)
C5 --- C6	1.430 (13)	O1---U1---N3	87.1 (3)
C6 --- C7	1.416 (14)	O2---U1---N3	93.7 (3)
C7 --- C8	1.406 (15)	O3---U1---N3	143.8 (2)
C8 --- C9	1.371 (18)	N1---U1---N3	151.4 (2)
C9 --- C10	1.379 (15)	O1---U1---N4	88.5 (3)
C6 --- C11	1.394 (14)	O2---U1---N4	88.4 (3)
O3---U1---N4	81.2 (2)	N3---C16---C17	116.6 (8)
O6---U1---N4	143.6 (3)	N4---C17---C16	115.4 (8)
N1---U1---N4	145.5 (2)	N4---C17---C18	121.7 (8)
N3---U1---N4	62.8 (2)	N4---C21---C20	123.7 (10)
U1---O3---C1	123.9 (6)	C1---C2---C3	109.2 (7)
U1---O6---C11	128.4 (6)	C2---C3---C4	113.0 (8)
U1---N1---C2	115.3 (5)	C2---N1---C5	118.1 (8)
U1---N1---C5	126.0 (6)	C5---C6---C7	116.9 (9)
U1---N3---C12	119.4 (6)	C6---C7---C8	119.9 (10)
U1---N3---C16	122.1 (6)	C6---C11---C10	118.9 (9)
U1---N4---C17	122.4 (6)	C7---C8---C9	119.3 (11)
U1---N4---C21	120.2 (6)	C8---C9---C10	122.0 (10)
O3---C1---O4	123.8 (9)	C11---C6---C5	123.1 (8)
O3---C1---C2	116.4 (8)	C11---C6---C7	120.0 (9)
O4---C1---C2	119.8 (9)	C11---C10---C9	119.8 (10)
O5---C4---N2	122.1 (9)	C12---N3---C16	117.9 (8)
O5---C4---C3	115.9 (8)	C12---C13---14	119.1 (9)
O6---C11---C6	121.5(8)	C13---C14---C15	119.4 (10)
O6---C11---C10	119.5 (9)	C14---C15---C16	118.4 (9)
N1---C2---C1	109.2 (8)	C15---C16---C17	121.2 (9)
N1---C2---C3	111.7 (8)	C16---C17---C18	122.8 (8)
N1---C5---C6	125.1 (8)	C17---N4---C21	117.4 (8)
N2---C4---C3	122.0 (9)	C17---C18---C19	119.8 (10)
N3---C12---C13	123.1 (9)	C18---C19---C20	119.3 (11)
N3---C16---C15	122.1 (9)	C19---C20---C21	118.0 (11)

Table (V – 3): Atomic coordinates for compound (**2**)

Atom	x /a	y / b	z / c
U1	0.8547(1)	0.5636(1)	0.5556(0)
O1	0.6311(10)	0.5138(5)	0.5414(3)
O2	1.0830(10)	0.6047(5)	0.5701(3)
O3	0.8940(9)	0.4413(5)	0.6262(3)
O4	0.7688(14)	0.3569(6)	0.6970(4)
O5	0.1771(12)	0.5811(7)	0.7096(4)
O6	0.7595(9)	0.7203(4)	0.5543(3)
O7	1.0116(12)	0.2029(6)	0.7054(4)
N1	0.7446(10)	0.6115(5)	0.6517(3)
N2	0.4321(11)	0.6227(5)	0.7600(3)
N3	0.8831(11)	0.5966(6)	0.4499(3)
N4	0.9958(11)	0.4242(6)	0.4947(3)
C1	0.7897(13)	0.4341(7)	0.6700(4)
C2	0.6849(13)	0.5284(6)	0.6875(4)
C3	0.4743(13)	0.5098(7)	0.6829(5)
C4	0.3612(13)	0.5766(6)	0.7207(4)
C5	0.7579(14)	0.6993(7)	0.6743(4)
C6	0.8124(12)	0.7878(6)	0.6452(4)
C7	0.8599(16)	0.8711(7)	0.6786(5)
C8	0.9157(17)	0.9604(8)	0.6528(6)
C9	0.9183(16)	0.9663(8)	0.5954(5)
C10	0.8672(14)	0.8872(7)	0.5618(5)
C11	0.8145(12)	0.7953(7)	0.5868(4)
C12	0.8214(13)	0.6835(7)	0.4288(4)
C13	0.8114(14)	0.7026(7)	0.3719(4)
C14	0.8651(16)	0.6301(8)	0.3348(5)
C15	0.9298(15)	0.5397(8)	0.3551(4)
C16	0.9361(15)	0.5255(7)	0.4136(4)
C17	1.0037(13)	0.4298(7)	0.4384(4)
C18	1.0704(16)	0.3515(7)	0.4060(7)
C19	1.1314(19)	0.2659(8)	0.4315(5)
C20	1.1232(19)	0.2586(9)	0.4891(15)
C21	1.0612(17)	0.3402(7)	0.5190(5)
C22	1.1566(21)	0.2162(10)	0.6675(6)

Table (V – 4): Hydrogen Atom coordinates for compound (**2**). Isotropic temperature parameters (U) are fixed at 0.08 $Å^2$.

H2	0.713	0.545	0.726
H2A	0.464	0.593	0.795
H2B	0.498	0.684	0.756
H3A	0.437	0.521	0.645
H3B	0.450	0.442	0.693
H5	0.729	0.705	0.713
H7	0.856	0.867	0.719
H7A	0.926	0.258	0.702
H8	0.951	1.017	0.675
H9	0.957	1.027	0.578
H10	0.867	0.894	0.522
H12	0.783	0.735	0.454
H13	0.767	0.766	0.359
H14	0.858	0.642	0.295
H15	0.969	0.488	0.330
H18	1.074	0.357	0.366
H19	1.179	0.212	0.410
H20	1.159	0.198	0.508
H21	1.065	0.337	0.559
H22	1.242	0.162	0.670
H23	1.220	0.277	0.676
H24	1.107	0.219	0.630

Table (V – 5): Anisotropic temperature factors for compound (**2**) ($Å^2$ x 10^3).

	U11	**U22**	**U33**	**U23**	**U13**	**U12**
U1	19(1)	21(1)	18(1)	-2(1)	1(1)	1(1)
O1	23(3)	23(3)	37(4)	1(2)	-1(3)	-1(3)
O2	25(3)	29(3)	27(4)	-2(3)	3(3)	-5(3)
O3	32(4)	26(3)	24(3)	-1(3)	1(3)	12(3)
O4	49(5)	38(4)	46(5)	8(4)	22(4)	11(4)
O5	34(4)	63(5)	48(5)	9(4)	5(4)	-4(4)
O6	29(3)	20(3)	32(3)	-7(3)	2(3)	7(3)
O7	33(4)	45(4)	55(5)	15(4)	4(4)	4(4)
N1	17(4)	20(3)	22(4)	1(3)	-2(3)	-2(3)
N2	18(3)	25(4)	18(3)	-6(3)	-4(3)	5(3)
N3	23(4)	27(3)	19(4)	4(3)	-3(3)	-3(3)
N4	24(4)	26(4)	22(4)	-2(3)	4(3)	10(3)
C1	18(4)	31(4)	28(5)	2(4)	3(4)	1(4)
C2	23(5)	19(4)	21(4)	1(3)	-3(4)	-2(3)
C3	19(5)	26(5)	41(6)	-3(4)	10(4)	-2(4)
C4	12(3)	26(4)	28(4)	1(3)	2(4)	6(4)
C5	26(5)	35(5)	15(4)	-6(4)	-4(4)	7(4)

C6	17(5)	20(4)	30(5)	-2(3)	5(4)	2(3)
C7	19(4)	33(5)	46(6)	-17(4)	-2(5)	1(4)
C8	30(5)	32(6)	57(7)	-6(5)	2(5)	-6(4)
C9	24(5)	28(5)	47(6)	2(4)	6(5)	-6(4)
C10	20(4)	30(4)	39(6)	3(4)	8(5)	10(4)
C11	19(5)	21(4)	32(5)	-3(3)	-2(4)	1(3)
C12	21(5)	21(4)	37(5)	1(4)	9(4)	-1(4)
C13	35(6)	27(4)	29(5)	9(4)	-6(4)	11(4)
C14	27(5)	46(6)	28(5)	11(4)	-5(5)	-5(5)
C15	16(4)	38(5)	30(5)	-12(4)	5(4)	-2(4)
C16	17(4)	22(4)	29(5)	-4(4)	1(4)	5(4)
C17	19(4)	28(4)	19(4)	-2(4)	-2(3)	2(4)
C18	32(5)	32(5)	23(5)	-6(4)	3(4)	2(4)
C19	46(7)	31(5)	49(7)	-13(5)	4(6)	19(5)
C20	61(8)	41(5)	28(6)	5(5)	11(6)	30(6)
C21	35(5)	26(4)	39(6)	5(4)	5(5)	14(4)
C22	45(7)	64(7)	47(7)	9(6)	13(7)	6(7)

The FAB mass spectra as well as ESI mass spectra of these complexes have proved to be valuable tools in assigning their molecular formulae (or definite fragments resulting from them) by the experimental value of m/z (most abundant isotopic mass) as well as matching between the experimental and simulated (calculated) isotopic distribution profile ; the simulated isotopic distribution profile has been obtained by a computer program developed by Prof. Y. Yan [46]. The FAB mass spectrum of (**3**) shows

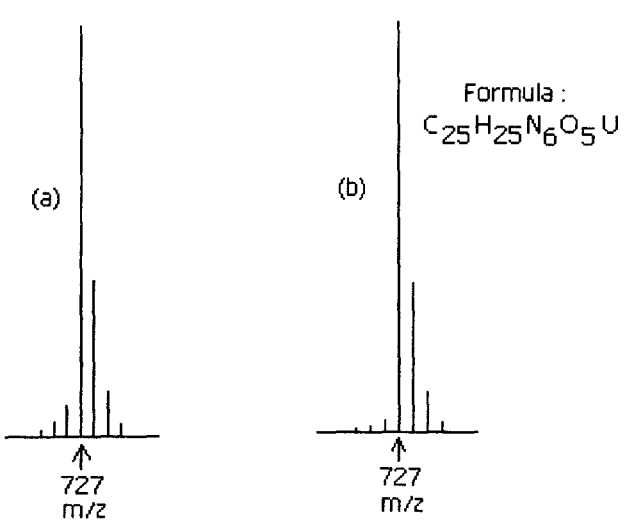

Fig.(V– 3):(a) FABMS data of (**3**) at the m/z (= 727) region corresponding to $[M–2H_2O+ H]^+$; (b) the calculated isotope pattern [46].

the characteristic isotopic distribution pattern in the region m/z = 727 [Figure (V – 3a)] corresponding essentially to the desolvated species $[M + H - 2H_2O]^+$ or $[UC_{25}H_{25}N_6O_5]^+$, where 'M' is the molecular formula of (**3**) (F.W. = 762). These data agreed with the corresponding theoretical value [Figure (V–3b)] thereby supporting the chemical composition of (**3**), along with its elemental analysis and other physicochemical data ; the same is true in other cases as well. In case of complex (**4**), the essentially intact molecular ion peak, $[M+3H]^+$ is observed at m/z = 997, and this assignment is verified through matching with the calculated data [Figure (V – 4)] ; here 'M' is the molecular formula of (**4**) (F.W. = 994). The noble aspect is that none of the extraspheric water molecules are lost during the mass spectral process, indicating their strong hydrogen bonding most likely with the amidine nitrogen atoms of the amino acid residue [Scheme (V – 1)]. In case of complex (**5**), the FAB mass spectrum shows the essentially intact desolvated species $[M+H-H_2O]^+$ at m/z = 699, where 'M' is the molecular formula of (**5**) (F.W.= 716). A good matching is observed with the corresponding simulated isotopic distribution

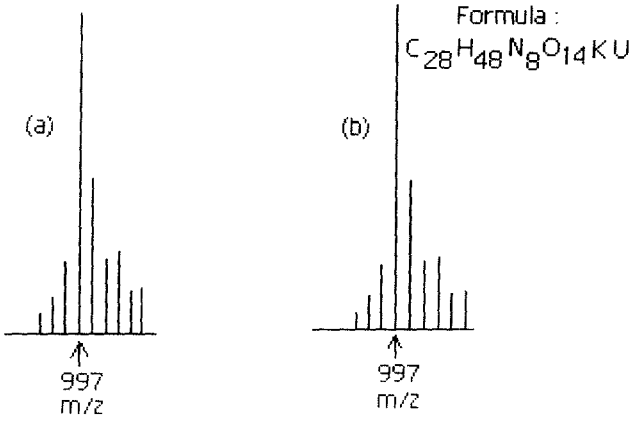

Fig.(V– 4): (a) FABMS data of (**4**) at the m/z (= 997) region corresponding to $[M + 3H]^+$; (b) the calculated isotope pattern [46].

pattern in this case as well [Scheme (V – 5)]. For complex (**6**) almost intact molecular ion peak, $[M+3H]^+$ is observed at m/z = 1263, where 'M' is the molecular formula of (**6**) (F.W.=1260). In Figure (V – 6) a tally between the experimental and calculated isotopic distribution pattern around m/z = 1263, is shown.

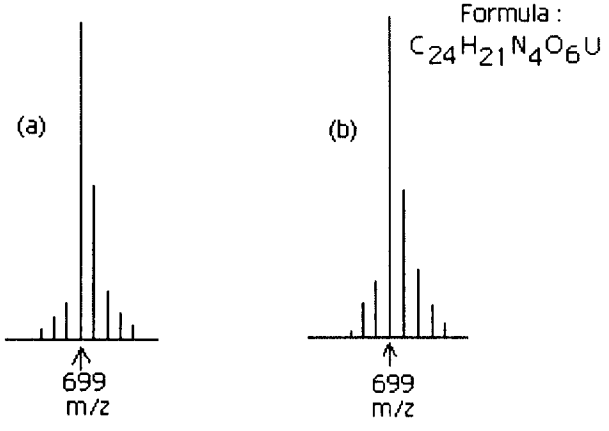

Fig.(V – 5): (a)FABMS data of (**5**) at the m/z (= 699) region corresponding to $[M–H_2O + H]^+$; (b) the calculated isotope pattern [46].

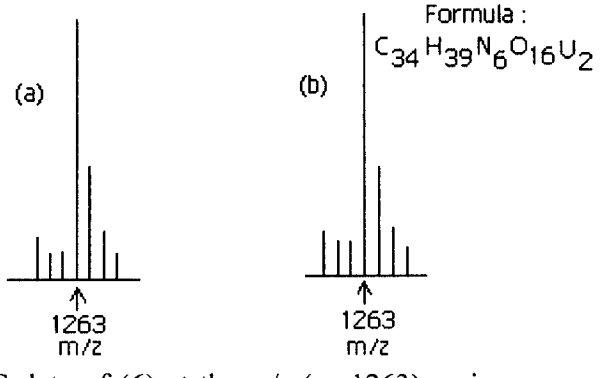

Fig.(V – 6): (a)ESIMS data of (**6**) at the m/z (= 1263) region corresponding to $[M + 3H]^+$; (b) the calculated isotope pattern [46].

The above– mentioned mass spectral data consistently indicate architectural stability of the present uranyl – aldimine ligand complexes where characterization is possible either for the essentially intact desolvated species in two cases or for the

complexes along with their extraspheric or intraspheric water molecules in other two cases. Their ability to retain this identity indicates stable nature of the UO_2^{2+} - aldimine ligand coordination ; this property is vital for the present kinetic studies where the size increase accompanying the electron transfer step $UO_2^{2+} \rightarrow UO_2^{+}$ is to be counterbalanced for a short duration for recording the relevant data.

The Λ_M [13.0 – 25 ohm^{-1} mol^{-1} cm^2, 301K, CH_3OH)] values for complexes **(2)**, **(3)**, **(5)** & **(6)** are consistent with their non-electrolytic formulation[43]. In case of compounds **(1)** and **(4)**, Λ_M (91.0 & 86.0 ohm^{-1} mol^{-1} cm^2, 301K, CH_3OH) values indicate their 1:1 electrolytic nature [43].

The IR spectrum of the free ligand [e.g., **(1)**] exhibits the ν (CH=N) band at 1635 cm^{-1} and it undergoes a red shift (by 20 cm^{-1}) in the corresponding complex **(6)** [85]; for other complexes [**(2)**, **(3)**, **(4)**, **(5)**] of this series, this ν (CH=N) band is located in the region 1620 – 1615 cm^{-1}. For the free ligand [e.g., **(1)**], the δ (OH) and ν(C – O) + δ(OH) modes of the phenolic – OH group appear at 1370 cm^{-1} and 1200 cm^{-1} respectively ; such bands disappear on chelation and the corresponding ν(C – O) mode of the phenoxide group is observed around 1210 cm^{-1} [155]. For this compound [OV – L – AsnHK **(1)**], the ν_{as} and ν_s modes of the carboxylate group are observed at 1615 cm^{-1} and 1410 cm^{-1} respectively ; these two bands appear at ca. 1600 cm^{-1} and ca. 1400 cm^{-1} respectively, for the present complexes with the Δν value ($\nu_{as} - \nu_s$ = 200 cm^{-1}) being in the range for unidentate carboxylate coordination [72]. The above data are in agreement with the X – ray structural data of **(2)** [Figure (V – 1)] regarding tridentate aldimine ligand coordination (involving the deprotonated phenolic – OH group, the azomethine nitrogen atom and are of the carboxylate oxygen atoms) for the present complexes.

The asymmetric stretching frequency (ν_3) of the UO_2^{2+} entity appears as a prominent band in the range 915 – 900 cm^{-1}, sometimes accompanied by a shoulder on the lower frequency side in all these cases [103].

On the basis of the above discussions, the schematic structural formulas of these complexes, as per Scheme (V – 2), may be adopted for further discussion.

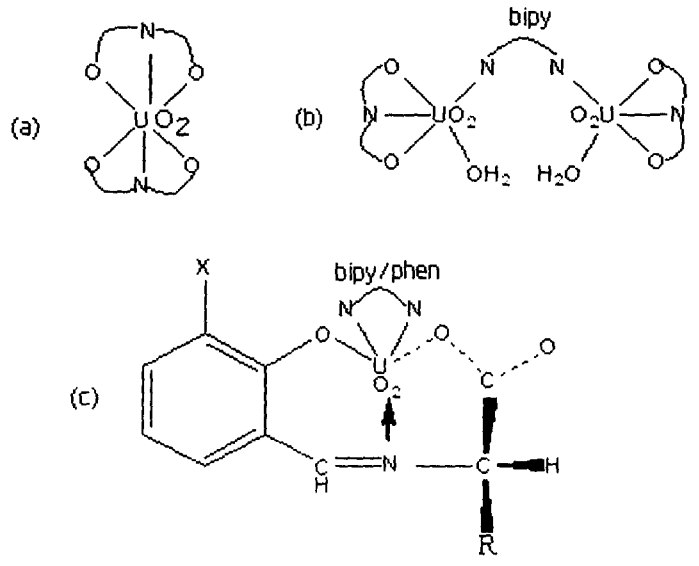

Scheme (V–2): Schematic structural formulas of the complexes; (a) complex (**4**); (b) complex (**6**) and (c) complexes (**2**), (**3**) & (**5**).

Now, the attention is focussed on the stereochemical aspect (both configurational and conformational factors) of these complexes on the basis of their chiroptical data, i.e., CD spectral data supported / substantiated by UV – VIS and ^{1}H NMR spectral data. Some of these data are reproduced here from reference 146 for lucid discussion ; such data together with the present X – ray structural, mass spectral and kinetic data will be published together comprehensively, as continued interest of this laboratory on chiral system [174]. This will help to rationalize their reactivity data (as discussed later). In the first stage we discuss the ^{1}H NMR spectral data of the ligand S – L – $ArgH_2$, its corresponding complex (**3**), the related complex (**4**) as well as that of complex (**3′**), [UO_2 (S – D – Arg)(phen)]. H_2O ; the last one contains the D – arginine

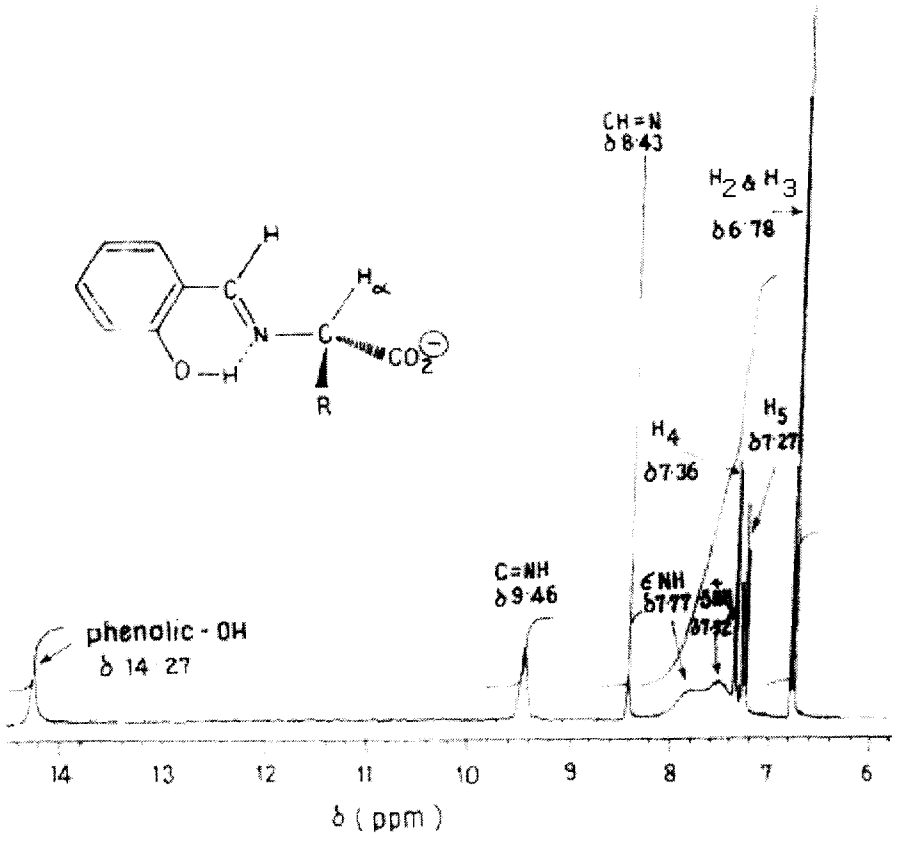

Fig.(V – 7): ^{1}H NMR spectrum of (S – L – $ArgH_2$) in DMSO – d_6. The schematic formula in the inset represents positive chirality, consistent with CD data [146].

residue and it is the quasi – enantiomer of (**3**) as evident from CD spectral data [Fig.(V – 12)] [146]. Some of the ^{1}H NMR spectral data have been recorded afresh to substantiate the data recorded earlier [146]; their interpretation have been checked here once again. The assignments of different ^{1}H NMR signals have been done on the basis of spin – decoupling experiments as well as 2D NMR data (^{1}H – ^{1}H cosy experiments). Scheme (V – 1) indicates the different proton designations of the ligand S – L – $ArgH_2$ in Figure (V – 7) which shows its ^{1}H NMR spectrum in DMSO – d_6 over the region δ 14.40 to δ 3.60 ppm and the data for the lower ppm range are summarized in Table (V – 6).

Table(V–6): Chemical shift (δ, ppm) values of major conformers of the ligands protons and those of the corresponding dioxouranium (VI) complexes along with the Δ (= $\delta_{complex} - \delta_{ligand}$) ppm values for the latter[146].

Free ligands / Compl -exes		Amino acid residue H_α	$H_{\beta 1}$	$H_{\beta 2}$	H_γ	H_δ	$-NH_2$	Aldehyde residue C_5 CH=N	OCH_3/H_5	H_4	H_2	H_3	bipy, phen parts [c] $H_{6'}$ $H_{2'}$ & $_{9'}$	$H_{5'}$ $H_{3'}$ & $_{8'}$	$H_{4'}$ $H_{4'}$ & $_{7'}$	$H_{3'}$ $H_{5'}$ & $_{6'}$
OV-L-AsnHK [b]		4.47	2.68	3.02[d]	-	-	-[e]	8.30	3.82		7.04	6.96 6.63	-	-	-	-
S-L-AsnHK . H_2O [b]		4.41	3.02	2.62[d]	-	-	-[e]	8.36		(7.64-7.24)[h]		(7.0-6.7)[f]	-	-	-	-
S-L-ArgH_2 [a, n]		3.78	1.75	1.92	1.49	3.10	7.77-7.52[l]	8.43	7.27		7.36	6.78[f]	-	-	-	-
OV-L-ArgHK [a, o]		3.87	1.77	1.90	1.49	3.11	7.74[m]	8.38	3.73		6.88[g]	6.53	-	-	-	-
(3)[a]	Δ	4.90	1.93		1.67	3.10		9.27		7.58[h]	7.00[j]	6.71	9.13	7.79	8.52	8.03
		1.12	0.015		0.18	0.00		0.84		0.26			0.03	0.08	0.06	0.05
(3′)[a]	Δ[k]	4.87	1.78	2.05	1.58	3.07		9.25		7.57	6.98	6.70	9.10	7.78	8.50	8.00
		1.09	0.03	0.13	0.09	-0.03		0.82		0.25			0.00	0.07	0.04	0.03
(4)[a]	Δ	4.87	1.90	2.12	1.67	3.12		9.12		3.99	7.14[g]	6.55	-	-	-	-
		1.00	0.13	0.22	0.18	0.01		0.74		0.26	0.26	0.02				
(5)[a]	Δ[i]	4.83	1.94	2.30	2.22	-	7.33 & 6.72	9.22		7.56[h]	6.98	6.7	9.11	7.78	8.5	8.0
		0.42						0.86					0.11	0.07	0.04	0.03
(6)[a]		5.29	2.56	2.78	-	7.23 & 6.87		9.22		3.94	7.13	6.59	7.22	8.69	7.46	7.95 8.39
	Δ	0.82						0.92		0.12	0.17	-0.04	0.18	0.06	0.11	0.10 0.08

[a] In DMSO – d_6 ; [b] In D_2O ; [c] δ ppm values for free bipy and phen protons have been obtained from references 99 and 100 ; [d] signals could not be resolved due to low solubility and their range is only given here ; [e] the $-NH_2$ protons have undergone exchange in D_2O ; [f] H_2 & H_3 signals are appearing together ; [g] H_2 & H_4 signals are appearing together ; [h] H_4 & H_5 signals are appearing together ; [i] Δ values for the S – L – $GlnH_2$ compound is calculated using the corresponding δ ligand values of S – L – AsnHK.H_2O ; [j] H_2 & C=NH proton signals appear together; [k] Δ values are calculated on the basis of the corresponding L- ligand (S-L-$ArgH_2$) data; [l] εNH(δ7.77) & ξNH_3^+ (δ7.52) signals ; [m] εNH& ξNH_3^+ signals appear together ; [n] ξ >C=NH signal appears at δ 9.96 ; [o] ξ >C=NH signal appears at δ 9.23 ; provide Scheme (V – 1) for different proton designations.

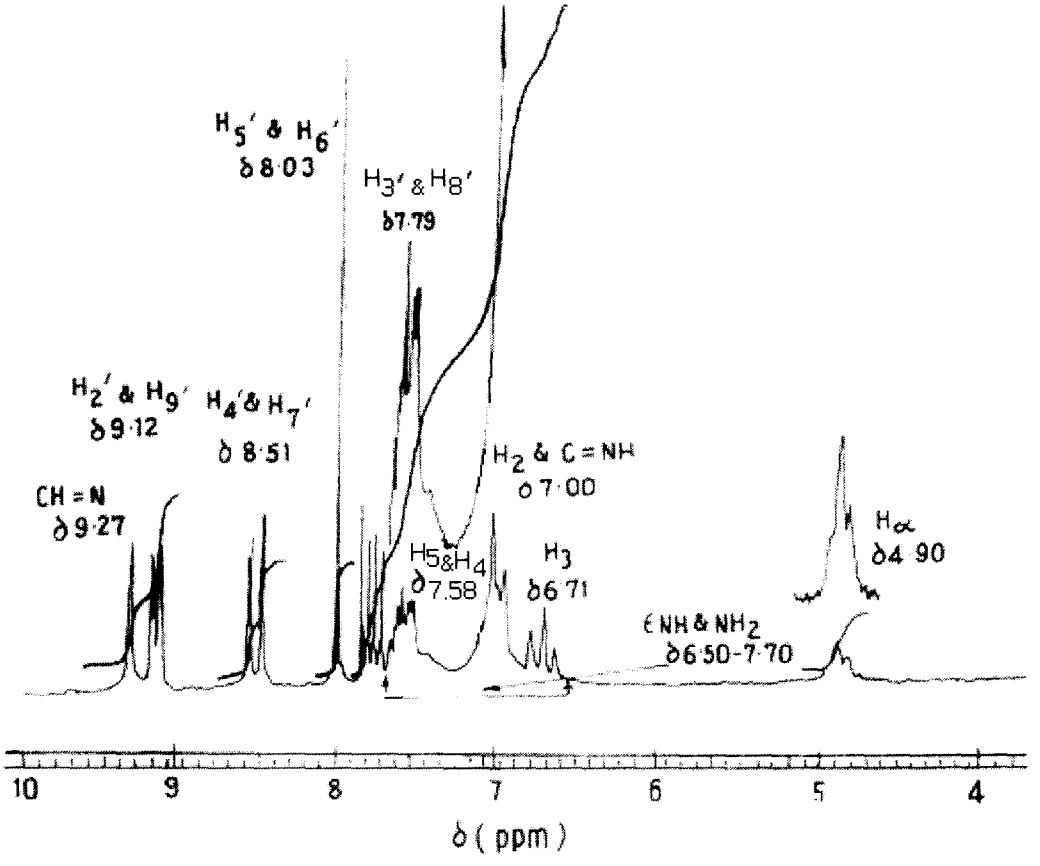

Fig.(V – 8): ^{1}H NMR spectrum of compound (**3**) in DMSO – d_6 [146] .

Figure (V – 8) shows the ^{1}H NMR spectrum of the corresponding complex (**3**), over the range δ 10.0 to δ 5.8 ppm, with the data for the lower ppm range being shown in Table (V – 6). A comparison of Figures (V – 7) and (V – 8) along with the Δ values (= $\delta_{complex} - \delta_{ligand}$) for the different proton signals in Table (V – 6), reveals several interesting features. In contrast to the strong deshielding effect (of δ 1.12 – δ 0.74 ppm) observed for the aldimine ligand protons situated around the immediate coordination zone [e.g., H_α and CH = N, Scheme (V – 1)], the 'phen' ring protons [Scheme (V–1) depicts the numbering system of different protons of the 1,10 – phenanthroline ligand] hardly undergo any deshielding effect [Table (V – 6)], although this bidentate nitrogen donor ligand is quite strongly coordinated to the UO_2^{2+} entity. The X – ray structural data of compound (**2**) [Figure (V – 1) and Table (V – 2)] illustrate this point involving the other bidentate nitrogen donor ligand (e.g., 2,2′ – bipyridyl) utilized in

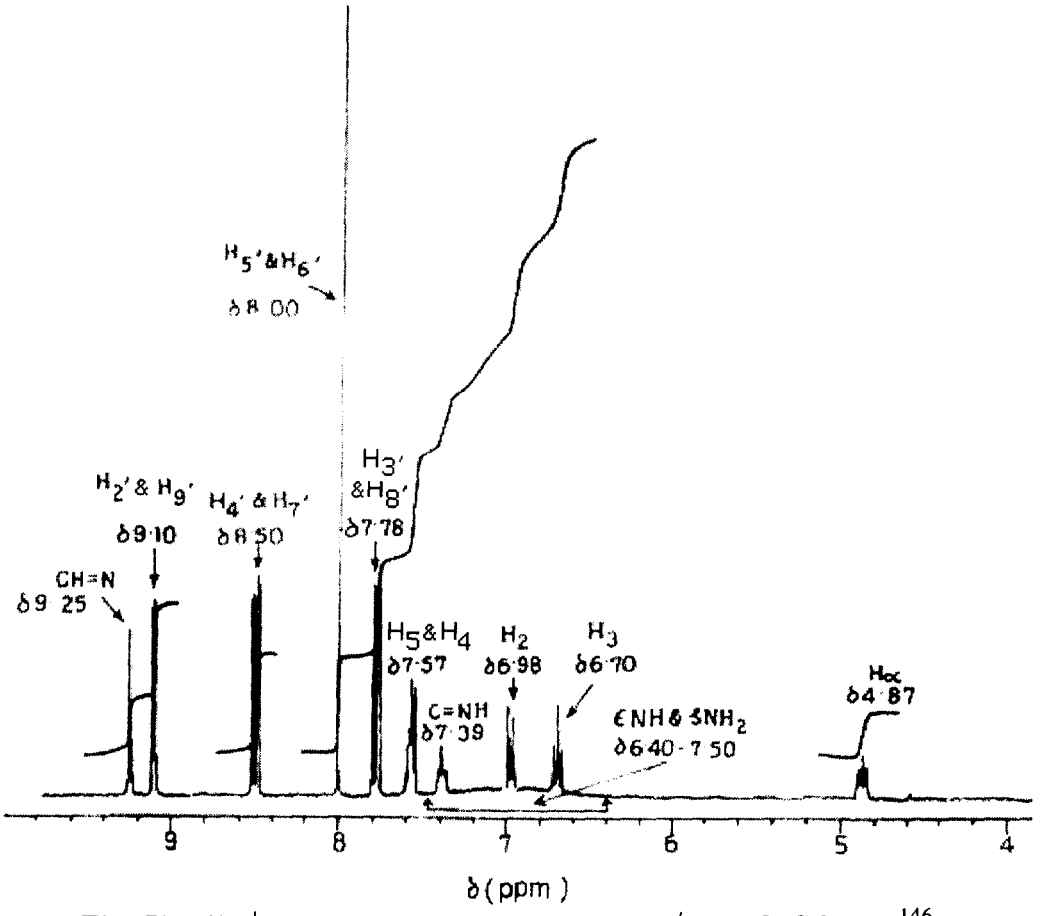

Fig.(V – 9): ^{1}H NMR spectrum of compound (**3'**) in DMSO – d_6 [146].

this study. Similar trend of low Δ values is observed for the 'bipy' ring protons in case of compound (**6**) as well [Table (V – 6)]. The strong deshielding of H_α and CH = N protons on coordination to the UO_2^{2+} entity, depends on several factors, e.g., drainage of electron density from the ligand through L → M σ bonding as well as magnetic anisotropy of the UO_2^{2+} entity [96]. On the other hand, extensive L → M π bonding occurs involving suitably disposed uranium orbitals and π^* orbitals of 1,10 – phenanthroline, thereby counterbalancing the deshielding effect through L → M σ bonding, leading to little change in Δ values of the 'phen' ring proton signals [Table (V – 6)]. The same is true for the Δ values of the 'bipy' ring protons of complex (**6**) {Table (V – 6)]. This electron withdrawing π – bonding influence is beneficial for studying the electron transfer process UO_2^{2+} → UO_2^{+} here, as it provides with a small time lag for recording the relevant absorption spectral data [Figure (V – 14b)] as stated later.

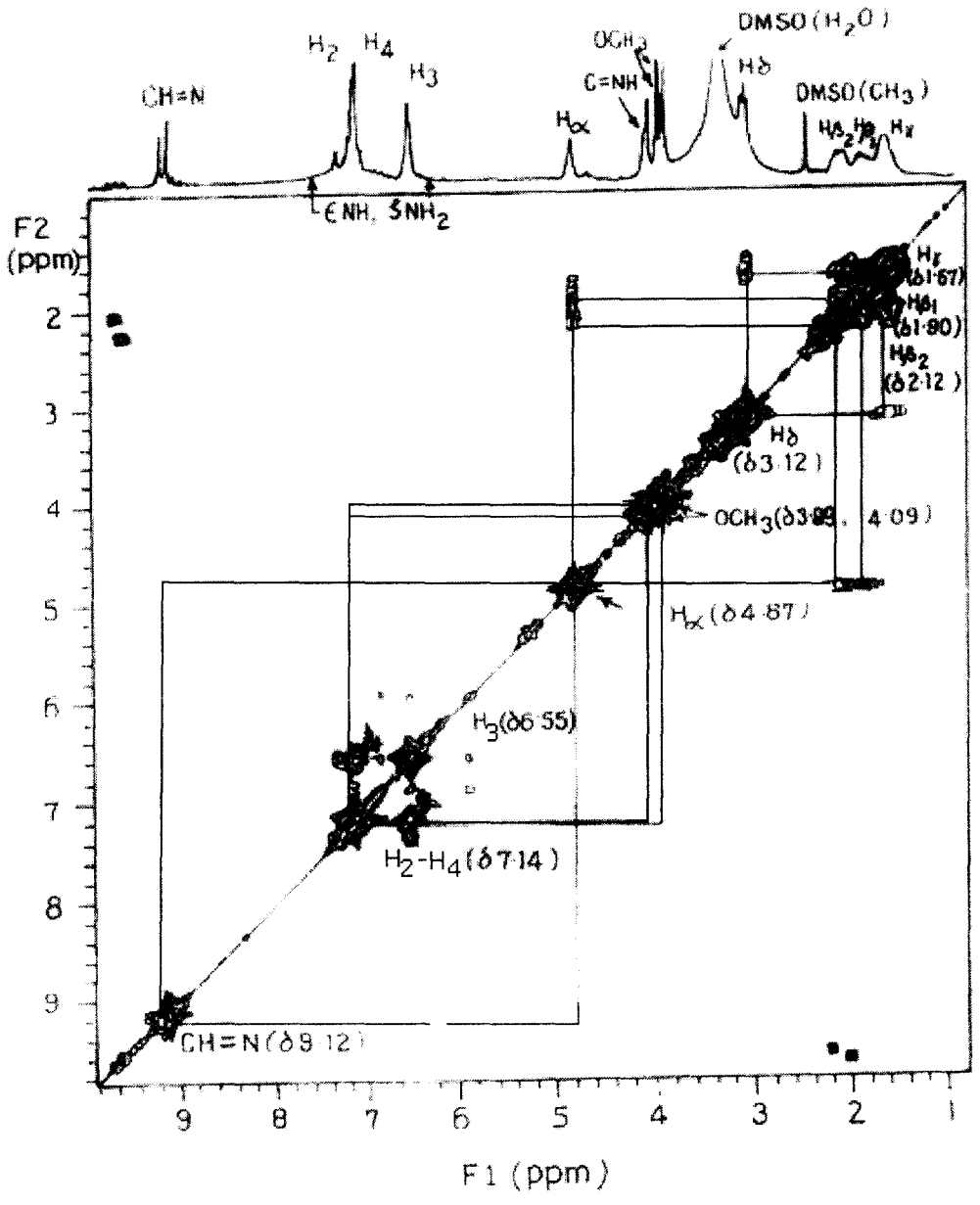

Fig.(V – 10): $^{1}H - {}^{1}H$ COSY spectrum (symmetrized) of compound (**4**) in DMSO – d_6 [146].

Another interesting aspect is revealed by comparing the ^{1}H NMR spectra of compounds (**3**) and (**3′**) in Figures (V – 8) and (V – 9) respectively. Although these two compounds have essentially identical chemical compositions, they deffer in the absolute configuration about the C_α atom [Scheme (V – 1)]. A closer look at the two above – mentioned ^{1}H NMR spectra reveals that for similar types of proton signals, small but distinct differences could be identified with respect to both their positions (δ ppm values) and multiplicities. This is mainly due to conformational differences of the 'R' part of the

amino acid residue in each case with respect to the chelate ring [conformer (b) in Scheme (V – 3) as shown later]. This is substantiated by their CD spectral data [Figure (V – 12)] where the two CD curves (briefly interpreted later) are almost mirror images to each other with respect to positions of CD maxima due to opposite configurations about the C_α atom [Scheme (V–1)], but intensity difference [$(\varnothing)_M$ values] exist due to the above – mentioned conformational differences.

Figure (V – 10) shows the 2D NMR spectrum of complex (**4**); it represents the procedure adopted here for assigning the different proton signals as well as the different spin – spin interactions existing here responsible for the observed multiplicities of the ^1H NMR signals, e.g., the long – range spin – spin interaction between the H_α and the azomethine (CH = N) protons [85, 107].

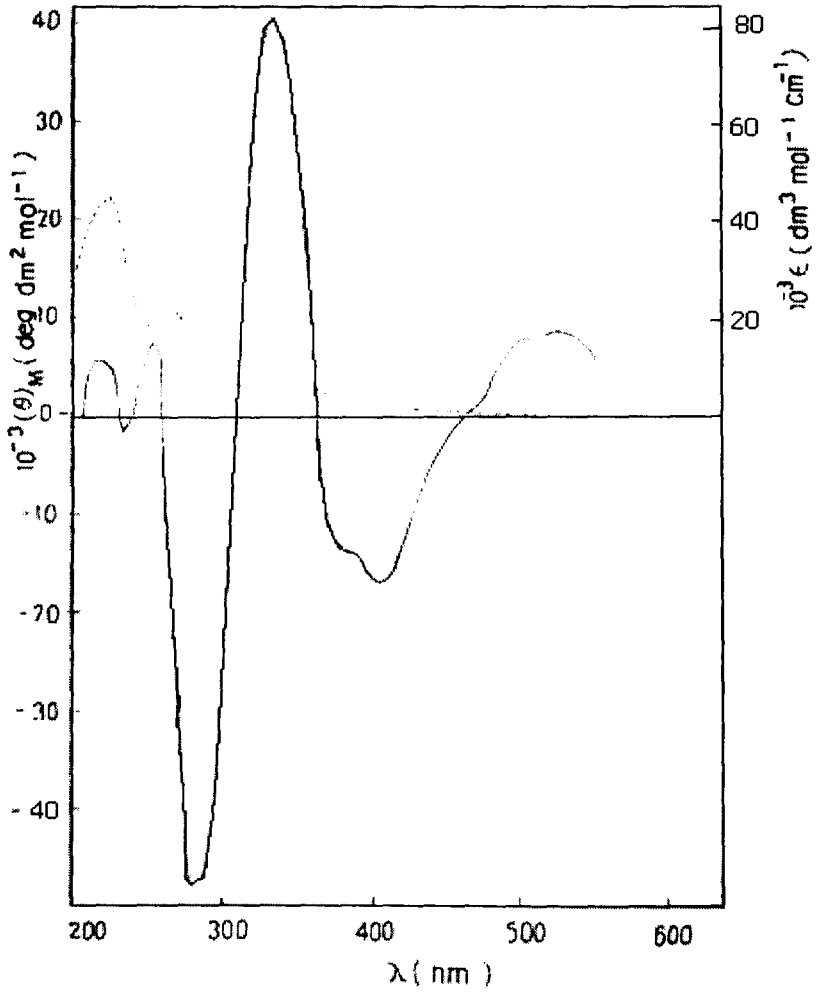

Fig.(V – 11): Electronic [-----] and CD [—] spectra of compound (**4**) in CH_3OH [146].

Presently, some of the relevant electronic absorption and CD spectral data [Figure (V – 11), (V – 12)] may be viewed in the light of existing guidelines for assigning absolute configuration / conformation of the pertinent ligands / complexes [79]. The quasi – enantiomeric nature of the CD curves of complexes (**3**) and (**3′**) in Figure (V–12) indicates the importance of absolute configuration of the amino acid residue in determining the overall chirality here [79].

In Figure (V – 11) the characteristic electronic spectral bands of complex (**4**) around 227 nm and 332 nm (sh) are assigned to $\pi \rightarrow \pi^*$ transitions of the O – vanillideneamino chromophore [Scheme (V – 3)] [79]. The band at 262 nm is due to a $n \rightarrow \pi^*$ transition of the azomethine group[79]. Another band extending from 355 nm to longer wavelength with diminishing intensity is assigned to charge transfer transition from the equatorial ligand $p\pi$ orbitals to the 5f / 6d orbitals of the uranium atom [Figure (V – 11)]. The relatively weaker apical oxygen $p\pi \rightarrow 5f$ transition within the UO_2^{2+} entity is observed by the aforesaid strong absorption occurring in the range 350 – 550 nm [96, 102, 203, 155]. However, the corresponding CD spectrum of complex (**4**) [Fig. (V– 11)] is helpful in resolving the two above electronic transitions by giving rise to two separate CD bands, e.g., a negative Cotton effect around 405 nm corresponding to the former equatorial ligand L → M charge transfer transition, while a positive Cotton effect around 530 nm characterizes the magnetically allowed intra oxometal transition [102, 155].

The typical couplet (S – shaped) CD band centred around 306 nm (with negative and positive maxima at 281 nm and 333nm respectively [Fig. (V – 12)] justifies the use of a coupled oscillator model [e.g., the salicylideneamino (SA) chirality rule [79]], for assigning the absolute configuration / conformation of the pertinent complexes. According to the SA chirality rule, for the N – salicylidene / orthovanillidene derivatives of aliphatic α – amino acids, this couplet CD band arises by transition moment dipole coupling of the carboxylate group (its $\pi \rightarrow \pi^*$ transition appears below 210 nm) with that of the aldimine chromophore [Scheme (V – 3)] and the positive Cotton effect (for L – type ligand system) around 320 – 330 nm is used here as the decisive one for chiroptical studies, as it usually undergoes only partial modification on coordination to a metal ion ; for the ligand S – L – $ArgH_2$ this positive CD band appears at 316 nm. According to the

above chirality rule, the sign of this 320 – 330 nm band can be predicted from the preferred chirality that the attachment band of the CO_2^- group has with the phenyl group methane carbon in the salicylidene / orthovanillidene chromophore. Positive chirality indicated by the 320 – 330 nm CD maximum can be represented by either conformer (a) or comformer (b), as per Scheme (V – 3).

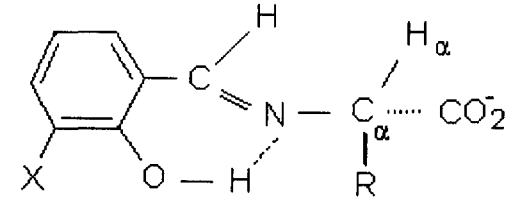

X = H / OCH_3 (a)

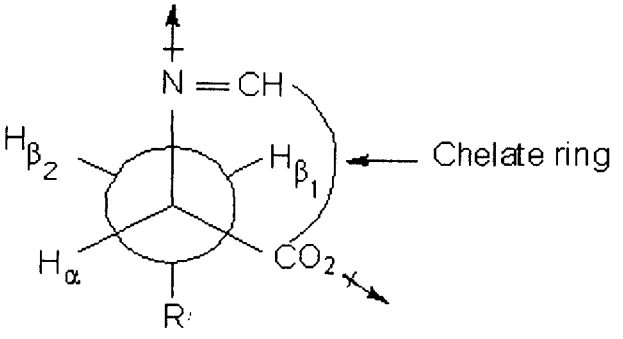

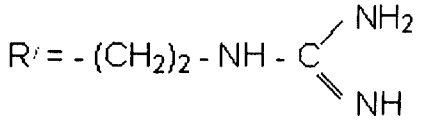

(b)

Scheme (V–3): Dominant conformers of aldimine ligands / complexes giving rise to positive chirality.

In case of conformer (a), the observer is looking along the C_α – N bond, with the CO_2^- group located on the right hand side ; the resultant of the two electric vectors (e.g., the CO_2^- group and the aldimine chromophore) is on the right – hand side of the observer which is correlated with positive CD maximum at 320 – 330 nm [79]. For conformer (b), contributions of the two above – mentioned electric vectors (indicated by arrows) give rise to a right – handed resultant, leading to the positive CD band at 320 – 330 nm. In case of aliphatic amino acids (including arginine), the contribution from the electric vector of R or R/ group [Scheme (V – 3)], is smaller than the two above – mentioned chromophores [79]. On the other hand, a left – handed CO_2^- group [Scheme

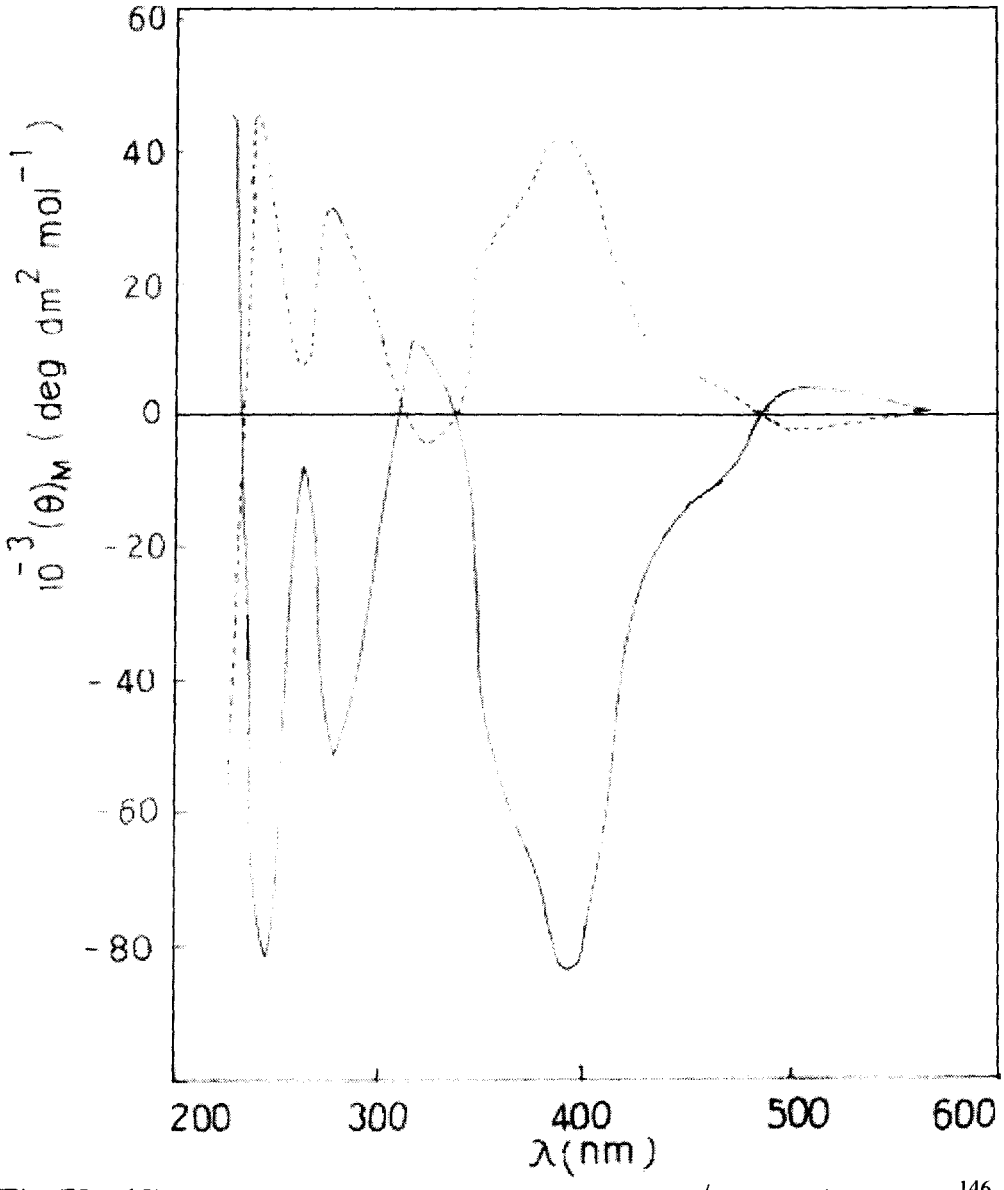

Fig.(V – 12): CD spectra of compounds (**3**) [—] and (**3′**) [------] in CH_3OH [146].

(V-3)] would have given rise to negative chirality with negative sign for the 320 – 333 nm CD band. Now viewing the two CD spectra in Figure (V– 12) in the above light, in case of complex (**3**) the positive CD maximum at 320 nm can be correlated with the configuration (C_α) of L – arginine residue, whereas for complex (**3′**) with D – arginine residue (possessing opposite configuration at C_α), a negative CD maximum is observed at 325 nm. However, the reduced intensity of these two CD bands [as compared to the 333 nm CD band in Figure (V – 11) is due to the opposite electric vector contribution from the $\pi \rightarrow \pi^*$ transition of the neutral donor ligand (1,10 – phenanthroline) [155].

As stated earlier, the essentially mirror image nature of the two CD curves in Figure (V – 12) with respect to band positions arise from opposite configurations of the two amino acid residues of the two complexes [(**3**) and (**3'**)] as well as stereospecific nature of the chelation process of the UO_2^{2+} entity with each aldimine ligand residue, leading to retention of configuration in each case. However, the difference in intensity between the two CD curves in terms of $(\varnothing)_M$ values in Figure (V – 12) can be traced to the conformational differences between the 'R' part of each amino acid residue. A comparison (proton signal by proton signal with respect to position and fine structure) of the two relevant ^1H NMR spectra [Figure (V – 8) and (V – 9)] support this view.

As evident from ^1H NMR spectra the extensive M → L π bonding occurs here in appropriate cases, involving suitably disposed uranium orbitals and π^* orbitals of the 'phen' ligand. This partial removal of electron density from the uranium orbitals as well as the compact donor set of ligands on the equatorial plane (as evident from X – ray structural data) can give the UO_2^+ entity some stability to be studied on both the spectrophotometric and the cyclic voltammetric time scale [equation (1b)]. Reaction stoichiometry study (discussed later) indicate the overall reaction as per equation (1).

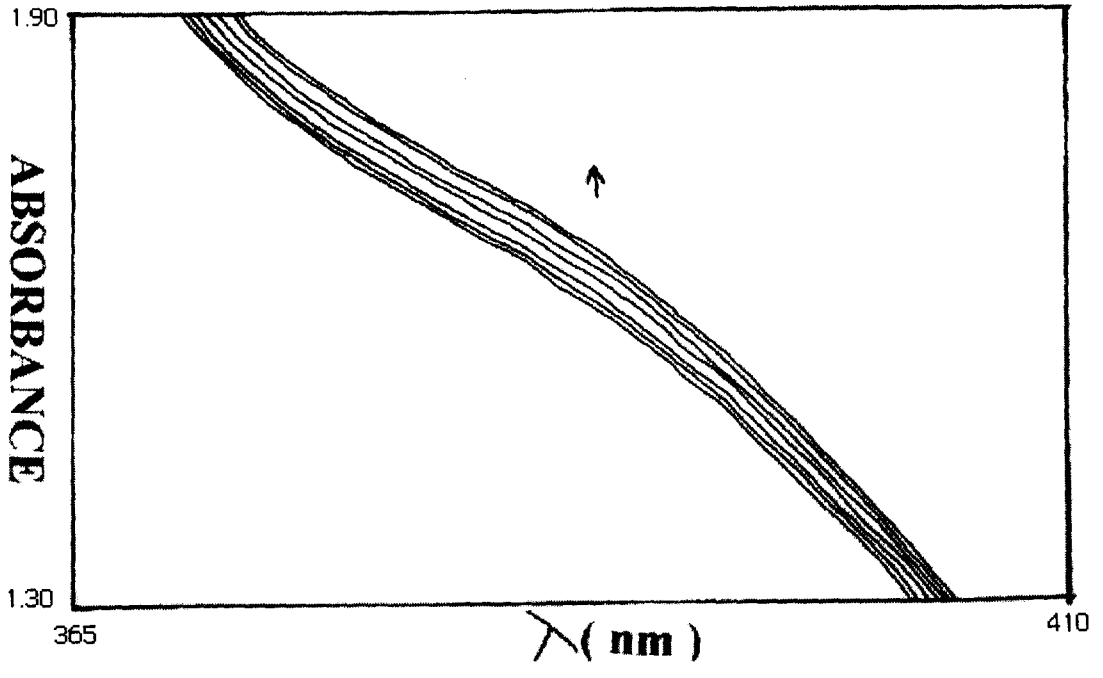

Fig.(V– 13): UV–VIS absorption spectral changes recorded every 20 seconds during the reaction of compound (**2**) [$1.12x10^{-3}$(M)] with Na_2SO_3 [$2.95x10^{-5}$(M)] in DMSO-H_2O (3 : 2, v/v) at 290 K.

$$(S^{IV}O_3)^{2-} + H_2O \rightleftharpoons (S^{VI}O_4)^{2-} + 2H^+ + 2e \quad \text{---} \quad (1a)$$

$$(U^{VI}O_2)^{2+} + e \longrightarrow (U^{V}O_2)^{+} \quad \text{---} \quad (1b)$$

$$(U^{V}O_2)^{+} + 2H^+ + e \longrightarrow U^{4+} + 2HO^- \quad \text{---} \quad (1c)$$

The overall reaction :

$$(U^{VI}O_2)^{2+} + (S^{IV}O_3)^{2-} + H_2O \longrightarrow U^{4+} + (S^{VI}O_4)^{2-} + 2HO^- \quad \text{---} \quad (1)$$

Reactivity of the present uranyl complexes towards Na_2SO_3 was studied in DMSO – H_2O (3 : 2 v/v) medium (purged with dinitrogen) spectrophotometrically [that is, recording of absorbance versus $\lambda_{(nm)}$ data every 20 seconds at 290 K, Figure (V–13)]. Distinct changes of absorbance with time occurred over the range 370 – 405 nm for complex (**2**) and other uranyl complexes of this series. From these data, the wavelength 383 nm was chosen for recording the time scan data (that is, for following the change of absorbance with time in order to calculate the rate constant data). At 290 K the change of absorbance with time [Figure (V – 14a)] during reaction with Na_2SO_3, is characterized by a single reduction step for complex (**3**). Interestingly, at a slightly lower temperature (288 K), the corresponding data [Figure (V – 14b)] represents a two – step reduction process, that is, a short – lived (ca. 65 seconds) intermediate could be detected in the first stage of reduction using the present conventional recording UV – VIS spectrophotometer. Most likely, Figure (V–14a) represents the overall two – electron reduction process as per equation (1), whereas Figure (V–14b) is able to distinguish between the two one – electron reduction steps ($UO_2^{2+} \rightarrow UO_2^{+} \rightarrow U^{4+}$) with the UO_2^{+} entity appearing as a short – lived intermediate as per equation (1b). Cyclic voltammetry and coulometry data of this complex (**3**) in DMSO medium [Figure (V–17) and (V–18)], support this inference[146]. This in agreement with the literature report on both thermodynamic and kinetic stability of the UO_2^{+} species in DMSO medium [141, 165]. Using this single step absorbance change versus time data as in Figure (V – 14a), the observed rate constant (k_{obs}, s^{-1}) were determined by least square method from the plots of log ($A_\alpha - A_t$) versus

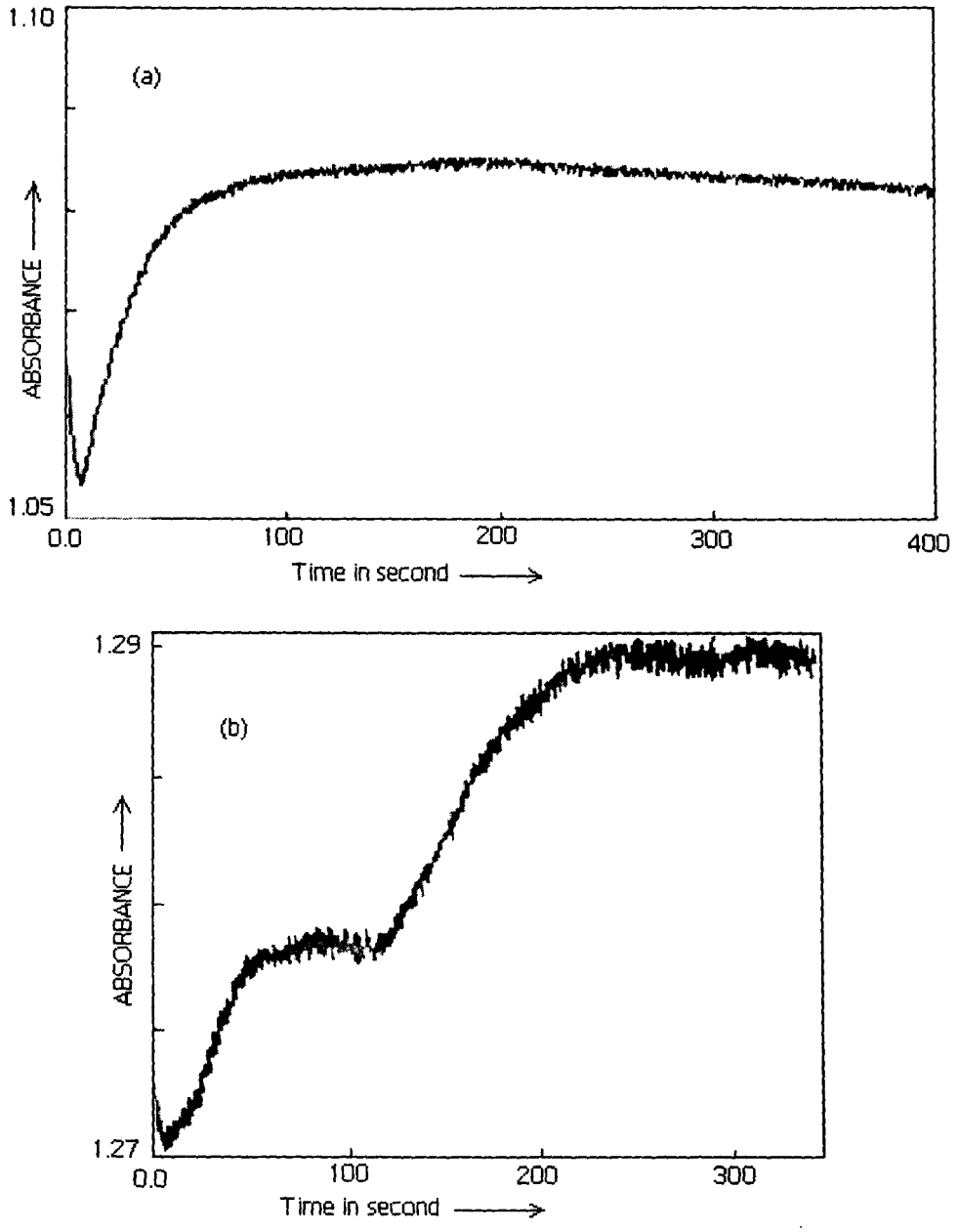

Fig.(V – 14): Monitoring of the change of absorption with respect to time (Time scan) for the reaction:- (a) between compound (**3**) [8.75×10^{-4} (M)] and Na_2SO_3 [1.75×10^{-5} (M)] in DMSO – H_2O (3 : 2, v/v) at 290 K and at λ = 383 nm ; (b) between compound (**3**) [8.75×10^{-4} (M)] and Na_2SO_3 [2.76×10^{-5} (M)] in DMSO – H_2O (3 : 2, v/v) at 288 K and at λ = 383 nm.

time, which were linear for nearly three half – lives. In the next stage, variation of the k_{obs} (s^{-1}) values was followed at a fixed Na_2SO_3 concentration with increasing concentration of each complex and from the linear plots [Figures (V–15), (V–16) showing some of them] of k_{obs} (s^{-1}) values versus complex concentration (M), the second order rate constants (k_2 M^{-1} s^{-1}) were obtained [Table (V–7)].

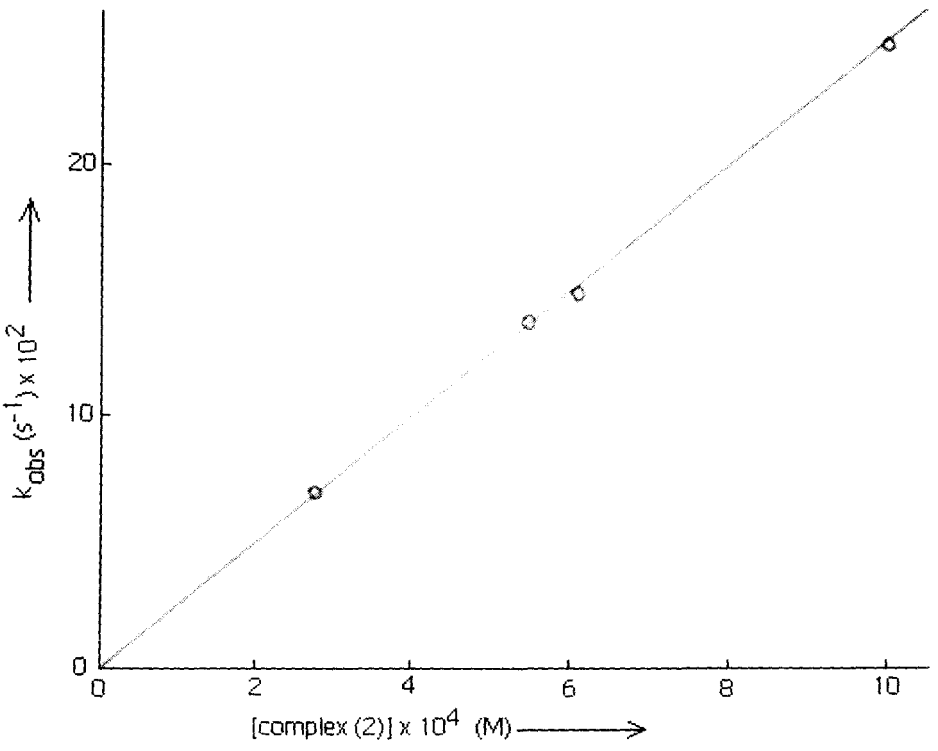

Fig.(V– 15)]: Dependence of the rate of reaction on the concentration of (**2**) with Na_2SO_3 [1x10^{-5} (M)] in DMSO – H_2O (3 : 2, v/v) at 290 K.

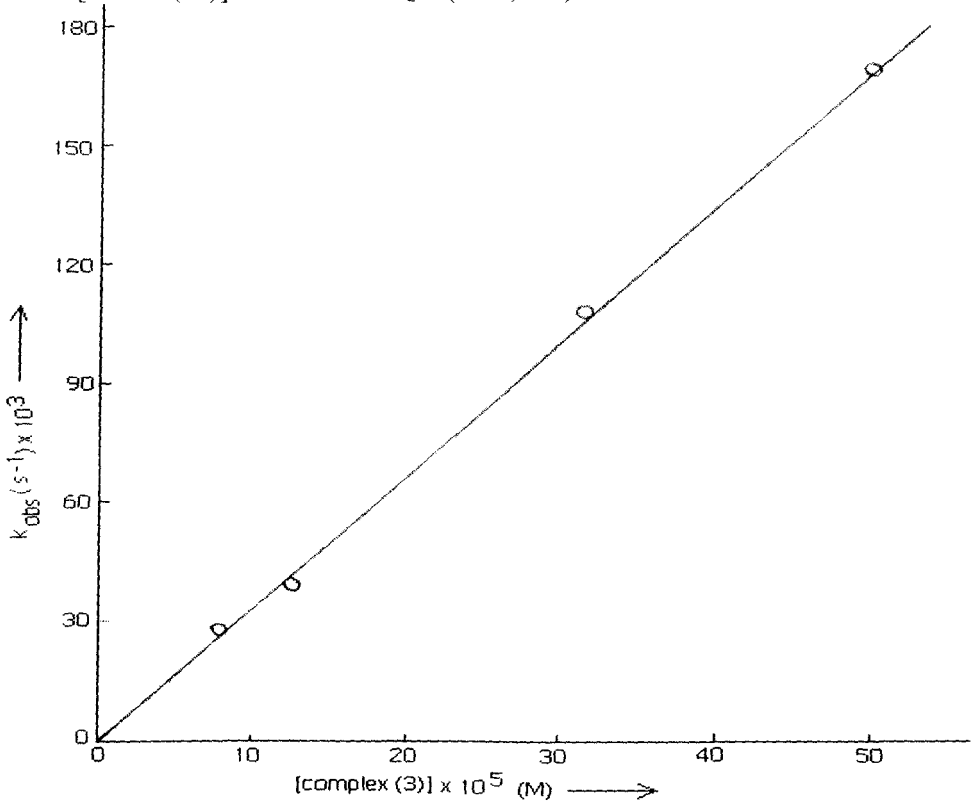

Fig.(V–16)]: Dependence of the rate of reaction on the concentration of compound (**3**) with Na_2SO_3 [1.0x10^{-5} (M)] in DMSO – H_2O (3 : 2, v/v) at 290 K.

Table (V–7): Kinetic data for the present uranyl complexes for the reaction with Na_2SO_3 [1.0×10^{-5} (M)] in DMSO – H_2O (3 : 2, v/v) at 290 K.

Complex No.	[Complex] (M) x 10^{-4}	k_{obs} (s^{-1}) x 10^{-2}	k_2 (M^{-1}, s^{-1}) * x 10^3
	2.76	7.10	
(2)	5.50	13.70	1.75
	6.10	14.90	
	10.0	24.70	
	0.78	2.80	
(3)	1.27	3.90	0.33
	3.17	10.80	
	5.0	16.90	
	1.55	88.50	
(3′)	3.62	50.20	1.86
	4.65	29.70	
	5.85	8.00	
	0.50	10.00	
(4)	0.69	11.80	1.80
	1.13	17.90	
	1.58	32.20	
	0.06	2.81	
(5)	0.11	5.50	5.45
	0.16	8.80	
	0.58	32.50	
	0.30	2.70	
(6)	2.01	22.90	1.12
	3.35	38.80	

* Derived rate constants from the plots of k_{obs} (s^{-1}) versus complex concentration [e.g., Figures (V-15), (V-16)].

Some important observations regarding these kinetic data are summarized below.

1. For evaluating the second order rate constants (k_2 M^{-1} s^{-1}) data, the concentration of the reducing agent (e.g., Na_2SO_3) was kept constant and the concentration of each complex was gradually increased over a range [e.g., Figures (V – 15), (V – 16)]. The alternative pathway, that is, increasing the concentration of Na_2SO_3 and keeping the

complex concentration fixed, could not be adopted here as the reactions become too fast at higher Na_2SO_3 concentration, to be followed by a conventional spectrophotometer.

2. For reactions between $NaHSO_3$ and $[Bu_4N]$ $[Mo^{VI}O_2(mnt)_2]$ in $CH_3CN - H_2O$ medium, saturation kinetics was observed for the dependence of k_{obs} (s^{-1}) values on $[HSO_3^-]$ [197], unlike the second – order kinetic behaviour in the present case.

In spite of the above difference in overall kinetic behaviour of the two systems (e.g., UO_2^{2+} and MoO_2^{2+}), the k_{obs} (s^{-1}) values for the present uranyl complexes are comparable in magnitude with those of $[Bu_4N]$ $[MoO_2(mnt)_2]$ [89, 104, 197]. Most likely, the closely related end products (that is, SO_4^{2-} or HSO_4^-) of these two reaction systems, decide the issue.

3. For the two – step reduction process at 288 K [Figure (V – 14b)], the k_{obs} (s^{-1}) values were calculated to be $26.1 \times 10^{-2}\ s^{-1}$ and $12.7 \times 10^{-2}\ s^{-1}$ for the first and second steps respectively.

The initial electron transfer step $UO_2^{2+} \rightarrow UO_2^+$ is followed by the relatively slower coupled electron and group transfer step $UO_2^+ \rightarrow U^{4+}$. Evidently, the overall two electron transfer coupled with oxygen atom transfer ($SO_3^{2-} + [O] \rightarrow SO_4^{2-}$), involves a short – lived UO_2^+ intermediate and could be detected here. This is in conformity with the ability of SO_3^{2-} ion to react with both one – electron and two – electron oxidants like Fe^{3+} and Cl_2 respectively [141, 165].

4. The second – order rate constants data of these complexes vary over a range [$k_2 = 0.33 - 5.45\ M^{-1}\ s^{-1}$, Table (V – 7)] reflecting their dependence on chemical compositions of the complexes, especially the donor atoms on the equatorial plane around the UO_2^{2+} entity as well as nature of the R groups of the amino acid residues. This is consistent with the inner – sphere nature of the overall electron transfer process [equation (1)] .

5. Another notable aspect is the kinetic behaviour of complex (**3'**) where the k_{obs} (s^{-1}) values measured as usual at a fixed Na_2SO_3 concentration, decrease with increasing complex concentration, unlike other complexes of this series [Table (V – 7)]. As per Scheme (V – 1), arrangement of the two substituents of C_α atom (that is the hydrogen atom, H_α and the R group) are interchanged for the D – arginine residue of complex (**3'**) as compared to that of the L – arginine residue of complex (**3**). The present inner – sphere electron transfer reaction [equation (1)] depend on the orientation of the R group around C_α [Scheme (V – 1)] in complexes (**3**) and (**3'**) as evident from the kinetic data in Table (V – 7) ; most likely electron transfer from the reducing agent (SO_3^{2-}) to the suitable orbital (HOMO) of the UO_2^{2+} entity in complex (**3'**) is hindered by the orientation of the R group, indicating configurational / conformational control of the electron transfer process [106, 155].

6. To establish reaction stoichiometry, a solution of complex (**2**) (0.08 g, 0.115 mmol) in 20 ml DMSO – H_2O (3 : 2 v/v) was treated with a solution of anhydrous Na_2SO_3 (0.38 g, 2.99 mmol) in 80 ml of the same solvent mixture, after thorough purging with dinitrogen. The reaction mixture was stirred under dinitrogen atmosphere at 301 K for 20 h. The organic part was extracted with CH_2Cl_2 and the sulphate (SO_4^{2-}) formed through the relevant reaction [equation (1)] was estimated as $BaSO_4$, giving 0.66 g (2.83 mmol) of $BaSO_4$ [89, 104]. As sulphite (SO_3^{2-}) oxidizes fairly rapidly in air, performing a blank experiment is essential for getting the reliable data about the amount of sulphate (SO_4^{2-}) formed in the pertinent reactions of the uranyl complexes [89, 104]. A blank experiment was performed under similar conditions, using the same amount (0.38 g, 2.99 mmol) of anhydrous Na_2SO_3 dissolved in same volume (100 ml) of the above solvent mixture ; 0.634 g (2.72 mmol) of $BaSO_4$ was obtained from the blank experiment. The difference between the two results, that is, 0.026 g (0.114 mmol) is the actual amount of $BaSO_4$ obtained, corresponding to the sulphate (SO_4^{2-}) formed through the reaction between complex (**2**) and Na_2SO_3. Therefore, almost 0.99 mol of sulphate was formed per mol of complex (**2**), during its reaction with Na_2SO_3 in accordance with equation (1).

Cyclic valtammetry and coulometry data in DMSO medium of a few of the present uranyl complexes are summarized here,[146] for complementing the above data on their redox activity towards Na_2SO_3, especially regarding the formation of the short – lived UO_2^+ intermediate. In the entire potential range of 0.0 to – 1.9 V, the free ligands display a reduction (E_{pc}) peak around – 1.60 V. For the present complexes the reductive response (E_{pc}) in the range of – 0.95 V to – 1.05 V can be assigned to a metal – centred process, involving reduction of the UO_2^{2+} entity. For example, in case of complex (**3**) [Figure (V – 17)] the catho – anodic peak system E_{pc} / E_{pa} is due to the one – electron transfer process [equation (1b & 1c)]. Controlled – potential coulometry [Figure (V – 18)] of this complex at – 1.15 V versus SCE indicates a 'n' value (number of electrons

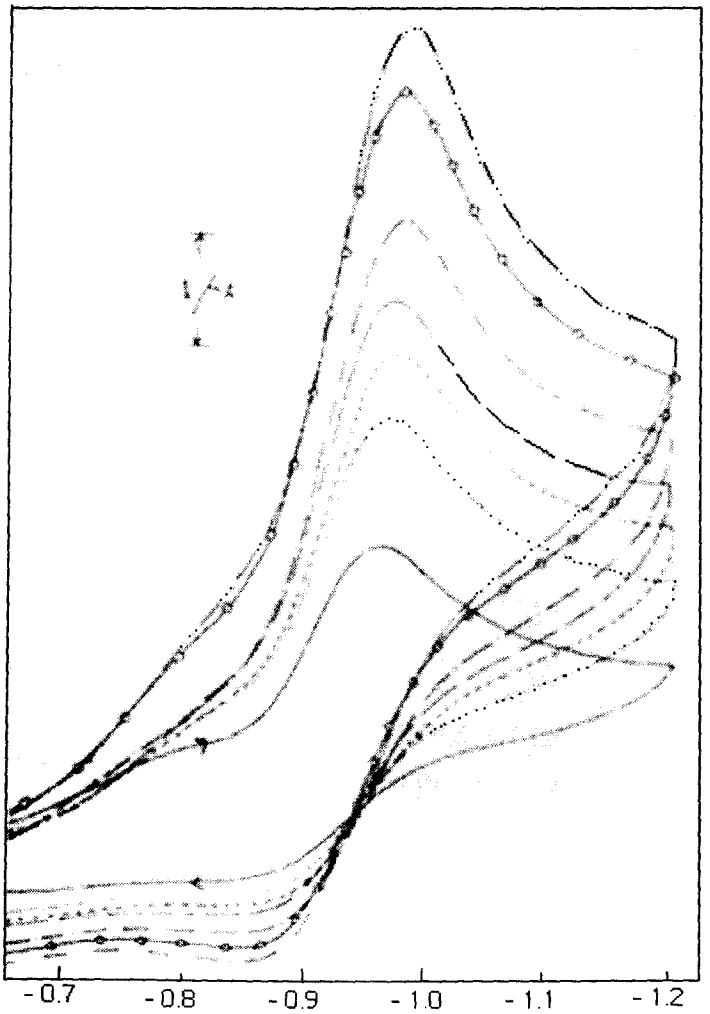

Fig.(V–17)]: Cyclic voltammogram of $[UO_2(S\text{-}L\text{-}Arg)(phen)].2H_2O$ (2.90 x 10^{-3} M) in DMSO with 0.1 M Bu_4NClO_4 ; scan rates : (i) 50 (—), (ii) 100 (·····), (iii) 150 (- - - -), (iv) 200 (– – –), (v) 250 (– – –), (vi) 300 (–o–o–), (vii) 350 (– · – · –) mVs^{-1}. Platinum working electrode [146].

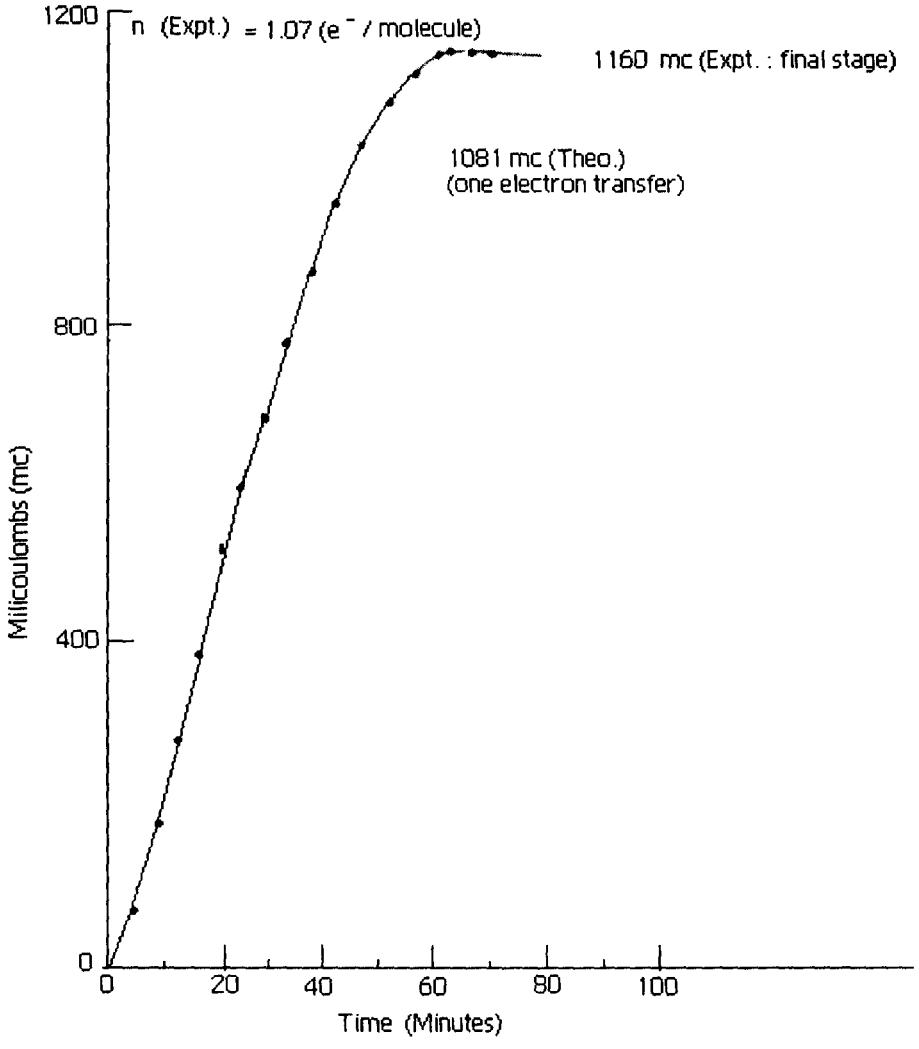

Fig.(V–18)]: Controlled – potential coulometry of $[UO_2(S\text{-}L\text{-}Arg)(phen)].2H_2O$ in 0.05M Bu_4NClO_4 / DMSO at a platinum plate electrode (4.2 cm x 2.2 cm) under N_2 at room temperature; electrolysis at – 1.15V vs SCE, using 11.2 μM of the substance [146].

transferred per molecule of complex) of 1.07, thereby confirming the formation of the UO_2^+ ion on the cyclic voltammetry and coulometric timescales in DMSO medium. In the cyclic voltammetric experiment [Figure (V – 18)], the forward scan generates the UO_2^+ species which undergoes solvation before start of the reverse scan and this is reflected by the departure of the peak – current ratio (i_{pc} / i_{pa}) from unity. The broad anodic peak becomes more prominent at faster scan rates ; ΔE_p value (E_{pa} - E_{pc}) increases upto 130 mV at a scan rate of 200 mVs^{-1} and remains constant beyond that limit. The corresponding quasi – enantiomeric complex (**3'**) containing the (S – D – Arg^{2-}) residue, exhibits different CD and ^1H NMR spectral response, as compared to those of complex

(**3**), due to configurational / conformational differences, as stated earlier. These differences are also reflected in the cyclic voltammetric data ; such data recorded at a scan rate of 50 mV s^{-1} for complex (**3**) indicate ΔE_p (mV) and (i_{pc} / i_{pa}) values of 90 mV and 1.64 respectively, as compared to the corresponding values of 130 mV and 1.55 for complex (**3'**). However, such differences are magnified to a large extent during redox reaction with Na_2SO_3, as evident from the relevant data in Table (V – 7) for these two complexes ; this aspect stresses the importance of the present kinetic studies, as they supplement not only the earlier cyclic voltammetric data but also substantiate the inference regarding configurational / conformational control of electron transfer reactions, in the present system. The compact equatorial donor set of ligands of the UO_2^{2+} entity contributed by the aldimine ligands, in conjunction with the M → L π bonding ability of the neutral bidentate donor (bipy / phen), provide some stability to the UO_2^{+} entity generated during the cyclic voltammetric process (cathodic reduction) and allow characterization of the one – electron process (UO_2^{2+} →UO_2^{+}) through coulometry [Figure (V–18)] [146]. In the absence of such compact donor set of ligands, e.g., for $UO_2(NO_3)_2$. $6H_2O$, cyclic voltammetric data in DMSO displays a single irreversible reduction wave [E_{pc} = - 0.52 V at a scan rate of 50 mVs^{-1} with similar conditions as in Figure (V – 17)] ; that is, the UO_2^{+} entity generated during the forward scan is completely decomposed through the post – chemical process (e.g., solvation) before starting the reverse anodic scan.

Figure (V–17) can be treated as a representative of the cyclic voltammetric data in DMSO medium of the present uranyl complexes where both the cathodic reduction (E_{pc}) and anodic oxidation (E_{pa}) peaks could be identified, with the latter type of peak becoming more prominent at faster scan rates.

Conclusion

Well – characterized uranyl complexes of aldimine ligands containing amino acid residues, have been utilized for studying their reactivities towards a suitable reducing agent like Na_2SO_3. Unlike the substrate saturation kinetics observed for the reaction of a MoO_2^{2+} - dithiolene ligand complex with HSO_3^- ion [197], the present uranyl complexes show linear dependence of k_{obs} (s^{-1}) values on complex concentration, i.e., they follow second – order kinetics [Figure (V–15), (V–16)]. The one – and two – electron reducing capability of Na_2SO_3 is utilized here for reactions with the pertinent uranyl complexes leading ultimately to the U^{4+} state [equation (1)], as verified through reaction stoichiometric studies. However, in case of complex (**3**) in DMSO - H_2O (3 : 2 v/v) medium at 288 K, the intermediate UO_2^+ state could be identified and k_{obs} (s^{-1}) value for the one – electron reduction process ($UO_2^{2+} \rightarrow UO_2^+$) could be calculated. These results are in agreement with the corresponding cyclic voltammetry and coulometry data [Figure (V – 17), (V – 18)]. The compact equatorial ligand donor set of ligands make it possible to resolve the overall 2 – electron transfer process into two one – electron reduction steps ($UO_2^{2+} \rightarrow UO_2^+ \rightarrow U^{4+}$) [Figure (V–14)] and help to stabilize the short – lived UO_2^+ intermediate for a time duration for its spectrophotometric characterization. Another interesting aspect is the difference in kinetic behaviour [Table (V–7)] between complexes (**3**) and (**3′**) containing the (S – L – Arg^{2-}) and (S – D – Arg^{2-}) residues respectively ; these data reflect the subtle configurational / conformational control via the relevant HOMO – LUMOs of the corresponding electron transfer processes [155].

The above data and inferences will surely substantiate the continued interest on the different facets of reactivity of the uranyl entity [176 - 178].
